Microscopic Analysis of the (^{3}He,t) and (^{3}He,^{3}He′) Reactions on 1p-Shell Nuclei*

GORDON C. BALL† AND JOSEPH CERNY
Lawrence Radiation Laboratory and Department of Chemistry, University of California, Berkeley, California 94720

(Received 29 July 1968)

The (^{3}He,t) and (^{3}He,^{3}He′) reactions on ^{9}Be, ^{12}C, ^{13}C, ^{14}C [(^{3}He,t) reaction only], ^{14}N, and ^{15}N have been investigated at ^{3}He energies varying between 40 and 50 MeV. Angular distributions were obtained for all prominent states up to excitations of 20 MeV. A microscopic analysis of these data has been carried out, using a local two-body interaction with an arbitrary spin-isospin exchange mixture. Spectroscopic factors were calculated, using intermediate-coupling wave functions for p-shell states, while simple j-j configurations were assumed for the levels which were populated by promoting a p nucleon to the s-d shell. A Yukawa interaction with a range of 1.2 F was found to give the best results. The strength of the effective *nucleon-nucleon* interaction required to fit these data is in good agreement with recent analyses of the (p,p') and (p,n) reactions on light nuclei. In particular, dominant $L=0$ transitions observed in the (^{3}He,t) reaction give values for the isospin-dependent ($V_{ST}=V_{01}$) and spin-isospin-dependent (V_{11}) terms (converted to an effective *nucleon-nucleon* interaction at a range of 1.0 F) of 20.6 and 16.5 MeV, respectively, while the strengths required to fit (^{3}He,t) $L=2,3$ transitions were generally enhanced. For inelastic transitions, the average strengths obtained for V_{00}, assuming a Serber exchange mixture, varied from 47.2 to 67.3 MeV, depending upon the L transfer involved. A comparison of the (^{3}He,t) and (^{3}He,^{3}He′) reactions populating analog final states (where $T_f=T_i+1$) is also presented. In general, these transitions were weak; however, it was possible to observe the lowest $T=\frac{3}{2}$ levels in the mirror nuclei ^{9}B-^{9}Be and ^{13}N-^{13}C, and several $T=1$ levels in ^{12}N-^{12}C.

I. INTRODUCTION

THERE has been a growing interest recently in the applications of a microscopic description to the inelastic and charge-exchange scattering of various projectiles by nuclei.[1–14] Utilizing the available experimental data from the (p,n) and (p,p') reactions, several attempts have been made to determine an effective nucleon-nucleon interaction in terms of a simple local potential with an arbitrary spin-isospin exchange mixture.[6–12] In particular, the population of ground and excited isobaric analog states in the (p,n) reaction provides a direct measurement of the isospin $V_{ST}=V_{01}$ and spin-isospin V_{11} terms in the effective two-body interaction, while the levels which are strongly populated in inelastic scattering are generally sensitive to the spin-

TABLE I. Energy levels observed in ^{12}N.

^{12}C(^{3}He,t)^{12}N				
Present work		Previous data[a]		Dominant shell-model configuration[a]
Energy (MeV±keV)	J^π	Energy (MeV±keV)	J^π	
0	1+	0	1+	$(p_{3/2})_{3/2}{}^7p_{1/2}$
0.96±20	2+[b]	0.969±7		$(p_{3/2})_{3/2}{}^7p_{1/2}$
1.20±30	(2−)[b]	1.198±9		p^7s
Not observed		1.65 ±80		p^7s
Not observed		(2.0 ±100)		
2.43±40[c]		2.35 ±80		p^8[b]
3.10±30		3.15 ±80		
3.50±40[c]		3.55 ±80		p^8[b]
4.24±50[d]				
5.27±40				

[a] See Refs. 41 and 42.
[b] Assignments made in present work.
[c] Angular distributions were not obtained for these levels.
[d] Broad level or group of levels.

* Work performed under the auspices of the U. S. Atomic Energy Commission.

† Present address: Chalk River Nuclear Laboratories, Chalk River, Ontario, Canada.

[1] R. M. Haybron and H. McManus, Phys. Rev. **136**, B1730 (1964); **140**, B638 (1965).
[2] V. A. Madsen and W. Tobocman, Phys. Rev. **139**, B864 (1965); N. K. Glendenning and M. Vénéroni, Phys. Letters **14**, 228 (1965); N. K. Glendenning, *ibid.* **21**, 549 (1966); A. Faessler, N. K. Glendenning, and A. Plastino, Phys. Rev. **159**, 846 (1967).
[3] N. K. Glendenning and M. Vénéroni, Phys. Rev. **144**, 839 (1966).
[4] G. R. Satchler, Nucl. Phys. **77**, 481 (1966).
[5] V. A. Madsen, Nucl. Phys. **80**, 177 (1966).
[6] W. S. Gray, R. A. Kenefick, J. J. Kraushaar, and G. R. Satchler, Phys. Rev. **142**, 735 (1966); M. M. Stautberg and J. J. Kraushaar, *ibid.* **151**, 969 (1966); M. M. Stautberg, J. J. Kraushaar, and B. W. Ridley, *ibid.* **157**, 977 (1967); M. M. Stautberg, R. R. Johnson, J. J. Kraushaar, and B. W. Ridley, Nucl. Phys. **A104**, 67 (1967); R. W. Barnard and G. D. Jones, *ibid.* **A106**, 497 (1968); **A108**, 655 (1968); **A111**, 17 (1968).
[7] M. B. Johnson, L. W. Owen, and G. R. Satchler, Phys. Rev. **142**, 748 (1966).
[8] G. R. Satchler, Nucl. Phys. **A95**, 1 (1967).
[9] W. G. Love and G. R. Satchler, Nucl. Phys. **A101**, 424 (1967),
[10] P. J. Locard, S. M. Austin, and W. Benenson, Phys. Rev. Letters **19**, 1141 (1967).
[11] C. Wong, J. D. Anderson, J. McClure, B. Pohl, V. A. Madsen and F. Schmittroth, Phys. Rev. **160**, 769 (1967).
[12] S. D. Bloom, J. D. Anderson, W. F. Hornyak, and C. Wong, Phys. Rev. Letters **15**, 264 (1965); J. D. Anderson, in *Isobaric Spin in Nuclear Physics*, edited by J. D. Fox and D. Robson (Academic Press Inc., New York, 1966) p. 530; C. Wong, J. D. Anderson, S. D. Bloom, V. A. Madsen, and F. Schmittroth, Lawrence Radiation Laboratory Report No. UCRL-70451, 1967 (unpublished).
[13] L. F. Hansen, M. L. Stelts, J. G. Vidal, and J. J. Wesolowski Lawrence Radiation Laboratory Report No. UCRL-70454, 1967 (unpublished); Bull. Am. Phys. Soc. **12**, 534 (1967); L. F. Hansen, M. L. Stelts, and J. J. Wesolowski, *ibid.* **13**, 632 (1968); L. F. Hansen, M. L. Stelts, J. G. Vidal, J. J. Wesolowski, and V. A. Madsen, Phys. Rev. **174**, 1155 (1968).
[14] J. J. Wesolowski, E. H. Schwarcz, P. G. Roos, and C. A. Ludemann, Phys. Rev. **169**, 878 (1968).

independent terms. So far, the (p,n) reaction has been reasonably successful in determining the strength of isospin-dependent terms[8,10–12]; however, the inelastic transitions generally give values for V_{00} which are enhanced due to collective or core polarization effects not accounted for by the wave functions of the initial and final states.[3,6–9]

One of the main purposes of this work was to employ the microscopic description in an analysis of the (^{3}He,t) and (^{3}He,^{3}He′) reactions on several $1p$-shell nuclei—specifically, ^{9}Be, ^{12}C, ^{13}C, ^{14}C, ^{14}N, and ^{15}N. These experiments were carried out at ^{3}He energies of 40–50 MeV and therefore the population of well-known levels up to an excitation energy of 15–20 MeV could be investigated. Some experimental studies of the (^{3}He,t) [13–16] and (^{3}He,^{3}He′) [17] reactions on light- and medium-weight nuclei have been reported previously. However, the relatively few microscopic analyses of these data have been generally limited to an investigation of the ground isobaric analog transitions observed in the (^{3}He,t) reaction on several light nuclei.[13,14]

In principle, an investigation of the (^{3}He,t) and (^{3}He,^{3}He′) reactions on $1p$-shell nuclei has several advantages which make it attractive for a microscopic analysis. First, many of the levels which are strongly populated in these reactions correspond to transitions which mainly involve the promotion of a single nucleon (i.e., almost pure single-particle transitions).[18] Second, the shapes and relative magnitudes of the angular distributions arising from single-particle transitions appear to fall into groups which depend not only on the orbital angular momentum transfer but also on the specific shell-model transition involved.[18] This effect has been very useful in utilizing the (^{3}He,t) reaction as a spectroscopic tool.[16] In particular, it was possible to make most probable spin and parity assignments for all levels observed in ^{14}O below 8 MeV.[18]

Finally, intermediate-coupling wave functions are available which have already been successful in predicting many nuclear properties for $1p$-shell states.[19] Although these wave functions are unable to predict the observed $E2$ transition rates without including an effective charge for the neutron,[20] the collective enhancement required is much less than that for heavier nuclei. As a result, the ability of a microscopic description to predict the shapes and relative magnitudes of the angular distributions for well-known p-shell transitions should provide a sensitive test of the applicability of a simple local potential for the inelastic and charge-exchange scattering of complex projectiles.

In the present analysis, distorted-wave Born approximation (DWBA) calculations have been performed using the microscopic description developed by Madsen.[5] Spectroscopic factors were calculated using the wave functions of Cohen and Kurath[19,21] for p-shell states, while simple j-j configurations were assumed for the levels which were populated by promoting a p nucleon to the s-d shell. The effective interaction was assumed to be a local Yukawa potential with an arbitrary spin-isospin exchange mixture. The strength of the effective nucleon-nucleon interaction required to fit these data is discussed in detail and also compared with the results obtained from recent (p,p'), (p,n),[6–12] and (^{3}He,t) [13,14] calculations.

Of additional interest in these experiments was the comparison of the (^{3}He,t) and (^{3}He,^{3}He′) reactions

TABLE II. Energy levels observed in the ^{12}C(^{3}He,^{3}He′)^{12}C reaction.

Energy (MeV±keV)[a]	$J^\pi; T$[b]	Dominant shell-model configurations[b]
0.0	0+; 0	$(p_{3/2})_0^8+(p_{3/2})_0^6(p_{1/2})_0^2$
4.43	2+; 0	$(p_{3/2})_{3/2}^7p_{1/2}$
7.65	0+; 0	$p^8+p^6(s,d)$
9.64	3−; 0	p^7d
10.84[c]	1−; 0	$p^7(s;d)$
11.83[c]	2−; 0	$p^7(s;d)$
12.71	1+; 0	$(p_{3/2})_{3/2}^7p_{1/2}$
14.08	4+; 0	p^8
15.11	1+; 1	$(p_{3/2})_{3/2}^7p_{1/2}$
16.11	2+; 1	$(p_{3/2})_{3/2}^7p_{1/2}$
16.57	2−; 1	p^7s
(17.26)[d]	1−; 1	p^7s
(17.77)[d]	0+; 1	p^8
18.40±60[e]	(; 1)[e]	
18.81[e]	2+; 1	p^8
(19.2)[d]	1−, 2−; 1	$p^7(s;d)$
19.58±60[f]	(; 1)[e]	

[a] Energy levels without error bars were well known previously (see Refs. 42–45).
[b] See Refs. 19, 40, 42–46.
[c] Angular distributions were not obtained for these levels.
[d] These levels were not observed in the (^{3}He,^{3}He′) reaction.
[e] Tentative assignments made in present work.
[f] Broad level or group of levels.

[15] H. E. Wegner and W. S. Hall, Phys. Rev. **119**, 1654 (1960); A. G. Blair and H. E. Wegner, Phys. Rev. Letters **9**, 168 (1962); M. E. Rickey, P. D. Kunz, J. J. Kraushaar, and W. G. Anderson, Phys. Letters **17**, 296 (1965); P. F. Donovan and P. D. Parker, Phys. Rev. Letters **14**, 147 (1965); R. Sherr, A. G. Blair, and D. D. Armstrong, Phys. Letters **20**, 392 (1966); N. Mangelson, M. Reed, C. C. Lu, and F. Ajzenberg-Selove, *ibid.* **21**, 661 (1966); N. Mangelson, F. Ajzenberg-Selove, M. Reed, and C. C. Lu, Nucl. Phys. **88**, 137 (1966); P. C. Rogers and H. E. Wegner, Phys. Rev. Letters **17**, 148 (1966); W. Whaling, Phys. Rev. **150**, 836 (1966); S. F. Eccles, H. F. Lutz, and T. S. Bohn, Lawrence Radiation Laboratory Report No. UCRL-50001-66-1, 1966 (unpublished), p. 13; L. G. Earwaker, Nucl. Phys. **A90**, 56 (1967); P. G. Roos, C. A. Ludemann, and J. J. Wesolowski, Phys. Letters **24B**, 656 (1967).

[16] R. H. Pehl and J. Cerny, Phys. Letters **14**, 137 (1965).

[17] See the following and references cited therein: J. Aguilar, W. E. Burcham, J. B. A. England, A. Garcia, P. E. Hodgson, P. V. March, J. S. C. McKee, E. M. Mosinger, and W. T. Toner, Proc. Roy. Soc. (London) **A257**, 13 (1960); E. R. Flynn and R. H. Bassel, Phys. Rev. Letters **15**, 168 (1965); R. J. Griffiths, Nucl. Phys. **A102**, 329 (1967); E. F. Gibson, J. J. Kraushaar, B. W. Ridley, M. E. Rickey, and R. H. Bassel, Phys. Rev. **155**, 1208 (1967).

[18] G. C. Ball and J. Cerny, Phys. Rev. **155**, 1170 (1967).

[19] S. Cohen and D. Kurath, Nucl. Phys. **73**, 1 (1965).

[20] A. R. Poletti, E. K. Warburton, and D. Kurath, Phys. Rev. **155**, 1096 (1967); G. A. Beer, P. Brix, H. G. Clerc, and B. Laube, Phys. Letters **26B**, 506 (1968).

[21] S. Cohen and D. Kurath, Nucl. Phys. **A101**, 1 (1967); D. Kurath (private communication).

TABLE III. Energy levels observed in ^{13}C and ^{13}N.

^{13}C			^{13}N			
^{13}C(^{3}He,^{3}He′)^{13}C (Present work) Energy (MeV±keV)	Previous data[a] Energy (MeV±keV)	J^π	^{13}C(^{3}He,t)^{13}N (Present work) Energy (MeV±keV)	Previous data[a] Energy (MeV±keV)	J^π	Dominant shell-model configuration[a]
0.0	0.0	$\frac{1}{2}-$	0.0	0.0	$\frac{1}{2}-$	$(p_{3/2})_0^8 p_{1/2}$
3.09	3.086±3	$\frac{1}{2}+$	2.37	2.366±2	$\frac{1}{2}+$	$(p_{3/2})_0^8 s_{1/2}$
3.68	3.681±3	$\frac{3}{2}-$	3.53±30	3.510±2	$\frac{3}{2}-$	$(p_{3/2})_{3/2}^7 (p_{1/2})_0^2$
3.85	3.852±3	$\frac{5}{2}+$		3.547±6	$\frac{5}{2}+$	$(p_{3/2})_0^8 d_{5/2}$
6.87	6.866±7	$\frac{5}{2}+$	6.38	6.382	$\frac{5}{2}+$	$p^8 s$
7.55±30	7.490±15	$\frac{7}{2}+$	7.17	7.166±8	$\frac{7}{2}+$	$p^8 d$
	7.550±15	$\frac{5}{2}-$	7.39	7.385±8	$\frac{5}{2}-$	$(p_{3/2})_{3/2}^7 (p_{1/2})_1^2$
8.86±30	8.86 ±20	$\frac{1}{2}-$	8.92±40	8.90 ±40	$\frac{1}{2}-$	$(p_{3/2})_{3/2}^7 (p_{1/2})_1^2$
9.50±30[b]	9.503±15	$(\frac{3}{2}-)$	[c]	9.48	$\frac{3}{2}-$	
[c]	11.078±20	$(\frac{1}{2}-)$	10.78±40[b]	10.80 ±30	$\frac{1}{2}-$	p^9
11.84±30	11.80 ±30	$\frac{3}{2}-$	11.85±40	11.87 ±30	$\frac{3}{2}-$	$(p_{3/2})_{3/2}^7 (p_{1/2})_1^2$
15.11[b]	15.113±5	$\frac{3}{2}-, T=\frac{3}{2}$	15.07	15.068±8	$\frac{3}{2}-, T=\frac{3}{2}$	$(p_{3/2})_{3/2}^7 (p_{1/2})_0^2$
			15.98±50[b]	15.96 ±50		

[a] See Refs. 36, 40, 43, 44, 47–49.
[b] Angular distributions were not obtained for these levels.
[c] These levels were weakly populated (see Fig. 3).

populating analog final states, where $T_f = T_i + 1$. In general, these transitions were weakly populated; however, it was possible to observe the lowest $T = \frac{3}{2}$ levels in mass 9 and 13 and several $T = 1$ levels in mass 12. As a result, a correspondence was established between seven excited $T = 1$ levels in ^{12}C and ^{12}N.

II. THEORY

The inelastic or charge-exchange scattering of various projectiles by nuclei can be described using either a collective or a microscopic model. Both of these descriptions generally utilize the DWBA expression for the transition amplitude given by[22]:

$$T = \int \chi_f^{(-)*}(\mathbf{k}_f, \mathbf{R}') \langle \Psi_f | V | \Psi_i \rangle \chi_i^{(+)}(\mathbf{k}_i, \mathbf{R}') d\mathbf{R}', \quad (1)$$

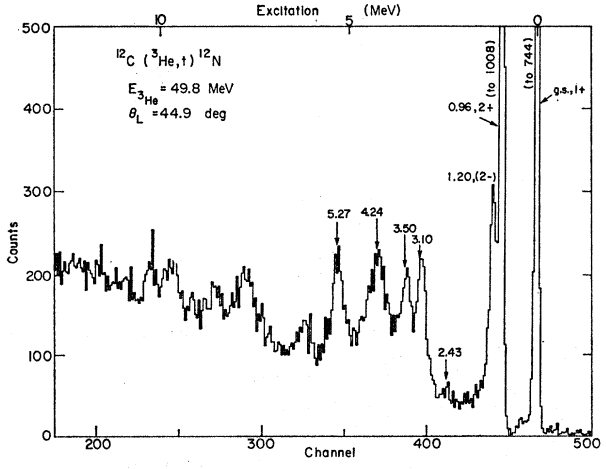

FIG. 1. Energy spectrum of the ^{12}C(^{3}He,t)^{12}N reaction at a ^{3}He energy of 49.8 MeV.

[22] G. R. Satchler, Nucl. Phys. 55, 1 (1964) and other references given there.

where $\mathbf{R}'$ is a vector between the c.m. of the projectile and the c.m. of the target nucleus. The $\chi_i^{(+)}$ and $\chi_f^{(-)}$ are distorted waves which describe the elastic scattering in the entrance and exit channels while the remaining factor represents the matrix element of the effective interaction taken over all nuclear coordinates of the initial and final states.

Until recently, the collective model was extensively used to describe inelastic scattering[23] since it was known that the states which are strongly excited by inelastic scattering are also strongly coupled to the ground state by the electromagnetic field.[24] Although this macroscopic description has been successfully applied to strongly excited states which can be characterized as collective in nature, the information which is obtained concerning nuclear structure is limited and in general the model is not applicable to weakly excited levels. Charge-exchange reactions have also been described in terms of an optical potential model in which the ground isobaric analog (quasi-elastic) transition results from an isospin or symmetry term in the optical potential,[25–27] while the radial derivative of this symmetry term gives rise to quasi-inelastic transitions.[27,28]

If a microscopic description is used, the nuclear wave functions Ψ_i and Ψ_f in Eq. (1) are expressed in terms of

[23] R. H. Bassel, G. R. Satchler, R. M. Drisko, and E. Rost, Phys. Rev. 128, 2693 (1962); E. Rost, *ibid.* 128, 2708 (1962); B. Buck, *ibid.* 130, 712 (1963); G. R. Satchler, R. H. Bassel, and R. M. Drisko, Phys. Letters 5, 256 (1963).
[24] B. L. Cohen and A. G. Rubin, Phys. Rev. 111, 1568 (1958).
[25] A. M. Lane, Phys. Rev. Letters 8, 171 (1962); Nucl. Phys. 35, 676 (1962).
[26] J. D. Anderson, C. Wong, J. W. McClure, and B. D. Walker, Phys. Rev. 136, B118 (1964); R. M. Drisko, P. G. Roos, and R. H. Bassel, Oak Ridge National Laboratory Report No. ORNL-4122, 1966 (unpublished), p. 63.
[27] R. M. Drisko, R. H. Bassel, and G. R. Satchler, Phys. Letters 2, 318 (1962); G. R. Satchler, R. M. Drisko, and R. H. Bassel, Phys. Rev. 136, B637 (1964).
[28] C. Wong, J. D. Anderson, J. W. McClure, and B. Pohl, Phys. Rev. 156, 1266 (1967).

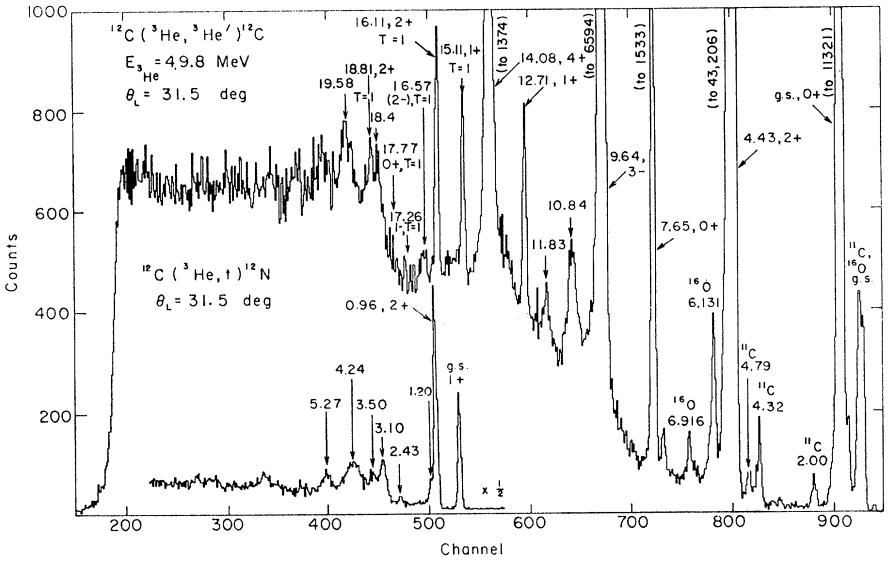

FIG. 2. Energy spectra of the ^{12}C(^{3}He,t)^{12}N and ^{12}C(^{3}He,^{3}He′)^{12}C reactions at a scattering angle of 31.5°. The ^{12}N spectrum has been adjusted to align the $T=1$ analog states populated in both reactions. The peaks corresponding to the g.s., 2.00-, 4.32-, and 4.79-MeV levels of ^{11}C represent an α contamination in the ^{3}He spectrum.

the motions of the individual target and projectile nucleons while the effective interaction is represented by a sum of two-body interactions between the projectile and target nucleons. In principle, this model is capable of describing all inelastic and charge-exchange transitions and also offers a means for testing nuclear wave functions providing the effective interaction is known.

For incident protons or neutrons at sufficiently high energies ($\geq$100 MeV) the impulse approximation is valid and the effective interaction can be replaced by the free nucleon-nucleon scattering amplitude.[1,29] However, at lower energies multiple scattering becomes more important and in addition the nucleon-nucleon scattering is modified by the presence of other target nucleons; therefore, the effective interaction is expected to be very complex. For simplicity, the effective interaction is generally restricted to be real, local and only dependent upon the distance between the projectile and target nucleons; however, an arbitrary spin-isospin exchange mixture is included. Hopefully, a consistent set of parameters can be obtained for the effective interaction provided the nuclear wave functions are well known.

One final restriction usually imposed in a microscopic description is to neglect the contributions from exchange processes in which the projectile nucleon (nucleons) is captured while a target nucleon (nucleons) is ejected; these effects will be discussed further later.

A. General Discussion of the Microscopic Model

Several theoretical formalisms convenient for discussion and calculation have been reported recently based on a microscopic description of the inelastic and charge-exchange scattering of various projectiles from nuclei.[3–5] The formalism developed by Madsen[5] has been used in the present work.

The effective interaction V in Eq. (1) can be expressed as a sum of projectile nucleon-target nucleon interactions given by

$$V=\sum_{p=1}^{a}\sum_{i=1}^{A}V(\mathbf{r}_p'-\mathbf{r}_i), \qquad (2)$$

where $\mathbf{r}_p'$ and $\mathbf{r}_i$ are the space coordinates of the projectile and target nucleons, and a and A represent the mass numbers of the projectile and target nuclei, respectively. If the wave function of the projectile is assumed to be a pure s state, then it can be factored into a part depending on space coordinates and a part

TABLE IV. Energy levels observed in ^{14}N.

^{14}N(^{3}He,^{3}He′)^{14}N Energy[a] (MeV±keV)	^{14}C(^{3}He,t)^{14}N Energy[a] (MeV±keV)	J^π, T[b]	Dominant shell-model configurations[b]
0.0	0.0	1+, 0	$(p_{1/2})^2$
2.31	2.31	0+, 1	$(p_{1/2})^2$
3.95	3.95	1+, 0	$(p_{3/2},p_{1/2})^{-1}$
4.91	4.91[c]	0−, 0	$(p_{1/2},s_{1/2})$
5.10	5.10	2−, 0	$(p_{1/2},d_{5/2})$
5.69	5.69	1−, 0	$(p_{1/2},s_{1/2})$
5.83	5.83	3−, 0	$(p_{1/2},d_{5/2})$
6.21[c]	6.21[c]	1+, 0	$(s_{1/2})^2$
6.44[c]	6.44[c]	3+, 0	$(s_{1/2},d_{5/2})$
7.03 (8.0–11.0)[d]	7.03 (8.0–9.5)[d]	2+, 0	$(p_{3/2},p_{1/2})^{-1}$
11.22±50[e]	10.43	2+, 1	$(p_{3/2},p_{1/2})^{-1}+(s,d)$
12.77±50[e]	12.49±40[c]		
	12.83±50[c]		
	13.70±40	1+, 1	$(p_{3/2},p_{1/2})^{-1}$

[a] Energy levels without error bars were well known previously.
[b] See Refs. 18, 40, 43, 44, 48, 50, 51.
[c] Angular distributions were not obtained for these levels.
[d] Several unresolved levels were populated in these regions (see Figs. 4, 5).
[e] Strong levels were also observed in the ^{14}N(α,α')^{14}N reaction (Ref. 56) at 11.3 and 12.9 MeV.

[29] A. K. Kerman, H. McManus, and R. M. Thaler, Ann. Phys. (N. Y.) 8, 551 (1959).

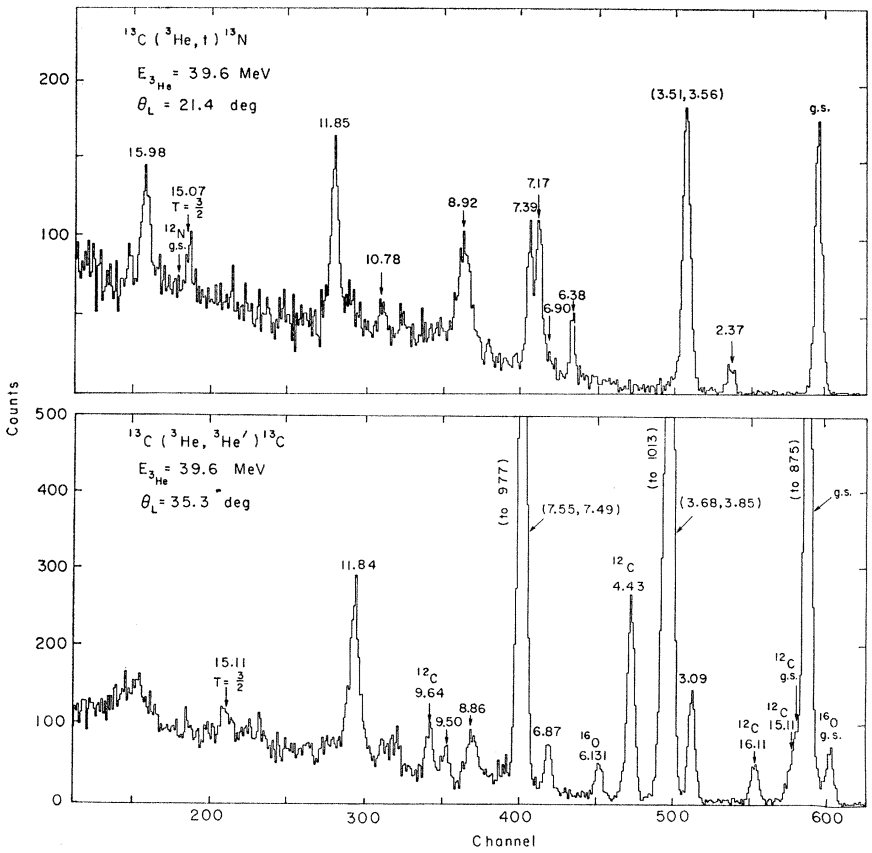

FIG. 3. Energy spectra of the ^{13}C(^{3}He,t)^{13}N and ^{13}C(^{3}He,^{3}He′)^{13}C reactions at a ^{3}He energy of 39.6 MeV. The spectra were recorded on separate analyzers with different gains. The peaks corresponding to the 15.11- and 16.11-MeV levels of ^{12}C represent an α contamination in the ^{3}He spectrum.

depending on spin-isospin coordinates. As a result, the nucleon-nucleon interaction $V(\mathbf{r}_p'-\mathbf{r}_i)$ can be expressed in terms of an effective *projectile-nucleon* interaction

$$\bar{V}(\mathbf{R}',\mathbf{r}_i)=\int d\xi' f^2(\xi')V(\mathbf{r}_p'-\mathbf{r}_i), \tag{3}$$

where $f(\xi')$ is the internal wave function of the projectile.

The nucleon-nucleon interaction is assumed to have the form

$$V(\mathbf{r}_p'-\mathbf{r}_i)=[V_{00}+V_{10}\boldsymbol{\sigma}_p\cdot\boldsymbol{\sigma}_i +\boldsymbol{\tau}_p\cdot\boldsymbol{\tau}_i(V_{01}+V_{11}\boldsymbol{\sigma}_p\cdot\boldsymbol{\sigma}_i)]g(\mathbf{r}_p'-\mathbf{r}_i), \tag{4}$$

where the strengths V_{ST} (for spin S and isospin T transfer) are expressed in MeV while the radial dependence $g(\mathbf{r}_p'-\mathbf{r}_i)$ is generally limited in calculations to functional forms which yield analytic expressions for the multipole expansion. In particular, the Gaussian

$$g(r)=\exp(-\beta r^2) \tag{5a}$$

and the Yukawa

$$g(r)=\exp(-\alpha r)/\alpha r \tag{5b}$$

are two suitable finite-range forms. In order to compare the strengths V_{ST} for potentials of different ranges and different strengths, Johnson *et al.*[7] suggest maintaining a constant volume integral of the potential

$$A_{ST}=V_{ST}\int g(r)dr, \tag{6}$$

where

$$\begin{aligned} A_{ST}&=V_{ST}\times(\pi/\beta)^{3/2}\text{: Gaussian,}\\ A_{ST}&=V_{ST}\times(4\pi/\alpha^3)\text{: Yukawa.}\end{aligned} \tag{7}$$

In order to compute the effective *projectile-nucleon* interaction, Eq. (3), the internal wave functions of the ^{3}He and triton projectiles are normally assumed to be Gaussian. If the nucleon-nucleon interaction, Eq. (4), is also chosen to be a Gaussian, then the resulting expression for $\bar{V}(\mathbf{R}',\mathbf{r}_i)$ is a Gaussian with a longer range and lower depth but the same volume integral, Eq. (7), as the nucleon-nucleon interaction.[5]

In the present analysis of the (^{3}He,t) and (^{3}He,^{3}He′) reactions, $g(r)$ was chosen to be a Yukawa interaction. As a result, the expression obtained for the effective projectile-nucleon interaction, Eq. (3), is very complex. Wesolowski *et al.*[14] have shown, however, that for large values of $(\mathbf{R}'-\mathbf{r}_i)$ this complicated expression can be approximated by a Yukawa with the same range α^{-1} but normalized strengths $\bar{V}_{ST}$ given by

$$\bar{V}_{ST}=V_{ST}\exp(\alpha^2/18\gamma^2), \tag{8}$$

where γ is proportional to the size parameter or average size parameters for the Gaussian wave functions of the

^{3}He and/or t projectiles [i.e., $\gamma=0.318$ and 0.291 for the (^{3}He,t) and (^{3}He,^{3}He′) reactions, respectively].[5] At a range of 1.0 F the simple Yukawa and the exact expression are almost identical for $|\mathbf{R}'-\mathbf{r}_i|\geq 3$ F and only deviate strongly at distances less than 2 F (i.e. $\approx 20\%$ at 2.0 F).[14] Since complex projectiles are strongly absorbed inside the nuclear surface, Eq. (8) can be expected to be reasonably correct; however, it should not be as accurate in the lighter nuclei due to their much smaller radii. In fact, the DWBA calculations performed for the (^{3}He,t) and (^{3}He,^{3}He′) reactions discussed herein were only insensitive to lower radial cutoffs ≤ 1.5 F. However, a comparison of the absolute strengths obtained in these experiments with those obtained in an analysis of the (p,p') and (p,n) reactions should provide a test of the validity of this approximation.

The expression for the differential cross section can be written as a coherent sum of single-particle transition amplitudes $F_{LM}{}^{j_1j_2}(\hat{k}_f)$:

$$\frac{d\sigma}{d\Omega}=\left(\frac{2\mu}{4\pi\hbar^2}\right)^2\frac{k_f}{k_i}\frac{1}{(2J'+1)(2J_i+1)}\sum_{JSLM}(2J+1)(2S+1)\Big|\sum_{j_1j_2T}D_{j_1j_2}(JSLT)\bar{V}_{ST}F_{LM}{}^{j_1j_2}(\hat{k}_f)(2L+1)^{-1/2}\Big|^2, \quad (9)$$

where

$$F_{LM}{}^{j_1j_2}(\hat{k}_f)=\langle\chi_f{}^{(-)*}(\mathbf{k}_f,\mathbf{R}')\,|\,Y_L{}^M(\hat{R}')g_L{}^{j_1j_2}(R')\,|\,\chi_i{}^{(+)}(\mathbf{k}_i,\mathbf{R}')\rangle,$$

$$g_L{}^{j_1j_2}(R')=\int \mathfrak{R}_{j_2l_2}(r_i)\bar{g}_L(R',r_i)\mathfrak{R}_{j_1l_1}(r_i)r_i{}^2dr_i,$$

and

$$D_{j_1j_2}(JSLT)=4(2j_1+1)^{1/2}(2j_2+1)^{1/2}\langle l_2\|Y_L\|l_1\rangle \times\begin{Bmatrix} j_1 & \frac{1}{2} & l_1\\ j_2 & \frac{1}{2} & l_2\\ J & S & L\end{Bmatrix}[\mathcal{S}(JJ_iJ_f;1T_iT_f;j_1j_2)\mathcal{S}'(SJ';1T')C'(T'T'1;P_i'-P_f')C(T_iT_f1;P_i-P_f)(-1)^{T'+T_i-P_i-P_f'} \times\delta_{P_i'-P_f',P_f-P_i}\delta_{T,1}+\mathcal{S}(JJ_iJ_f;0T_iT_f;j_1j_2)\mathcal{S}'(SJ';0T')\delta_{P_i'P_f'}\delta_{P_iP_f}(2T_i+1)^{-1/2}(2T'+1)^{-1/2}\delta_{T,0}]. \quad (10)$$

In the above expressions, the subscripts i and f label initial and final states; primes indicate projectile coordinates and quantum numbers; J, L, S, and T denote total, orbital, spin, and isospin transfer; the quantum numbers labeled P represent z components of isospin; and l_1,j_1 and l_2,j_2 represent the orbital and total angular momenta of the target nucleon in its initial and final states. The radial form factors $g_L{}^{j_1j_2}(R')$ are dependent upon the radial wave functions $\mathfrak{R}_{jl}$ of the bound particle in its initial and final state while the nuclear structure information is contained in the quantity $D_{j_1j_2}$, where $\mathcal{S}$,C and $\mathcal{S}'$,C' represent target and projectile spectroscopic factors and isospin Clebsch-Gordan coefficients, respectively.

As was mentioned previously, the levels which are strongly populated in the (^{3}He,t) and (^{3}He,^{3}He′) reactions on $1p$-shell nuclei correspond either to p-shell hole states or levels which have the configuration $1s^41p^{A-5}2s$ or $1s^41p^{A-5}2d$ (from here on we will assume a closed $1s$ shell and suppress all principal quantum numbers). Since simple j-j configurations will be assumed for the levels which are formed by promoting a p nucleon to the s-d shell, only one single-particle transition $j_1\rightarrow j_2$ contributes to the cross section. If intermediate-coupling wave functions are used for the p-shell states, then several different single-particle transitions (all with $l_1=l_2=1$) contribute. However, since the single-particle transition amplitudes $F_{LM}{}^{j_1j_2}$ were found to be relatively insensitive to the binding energies of the target nucleon in its initial and final states, $F_{LM}{}^{j_1j_2}$ was calculated only for the dominant single-particle transition predicted in the j-j limit. The validity of this approximation will be discussed later (see Sec. IV A3).

Since in the present analysis $F_{LM}{}^{j_1j_2}$ was computed for only one single-particle transition $j_1\rightarrow j_2$, the expression for the differential cross section, Eq. (9), can be written as

$$\frac{d\sigma}{d\Omega}=\sum_{JSL}\sigma(j_1j_2L\theta)\Big|\sum_T\frac{G(JSLT)}{\sqrt{\pi}}\bar{V}_{ST}\Big|^2, \quad (11)$$

where

$$\sigma(j_1j_2L\theta)=\left(\frac{2\mu}{4\pi\hbar^2}\right)^2\frac{k_f}{k_i}\sum_M|F_{LM}{}^{j_1j_2}(\hat{k}_f)(2L+1)^{-1/2}|^2, \quad (12)$$

and the nuclear structure factor $G(JSLT)$ is given by

$$G(JSLT)=\left[\frac{\pi(2J+1)(2S+1)}{(2J'+1)(2J_i+1)}\right]^{1/2}\sum_{j_1j_2}D_{j_1j_2}(JSLT), \quad \text{for } l_1=l_2$$

$$=\left[\frac{\pi(2J+1)(2S+1)}{(2J'+1)(2J_i+1)}\right]^{1/2}D_{j_1j_2}(JSLT), \quad \text{for } l_1\neq l_2. \quad (13)$$

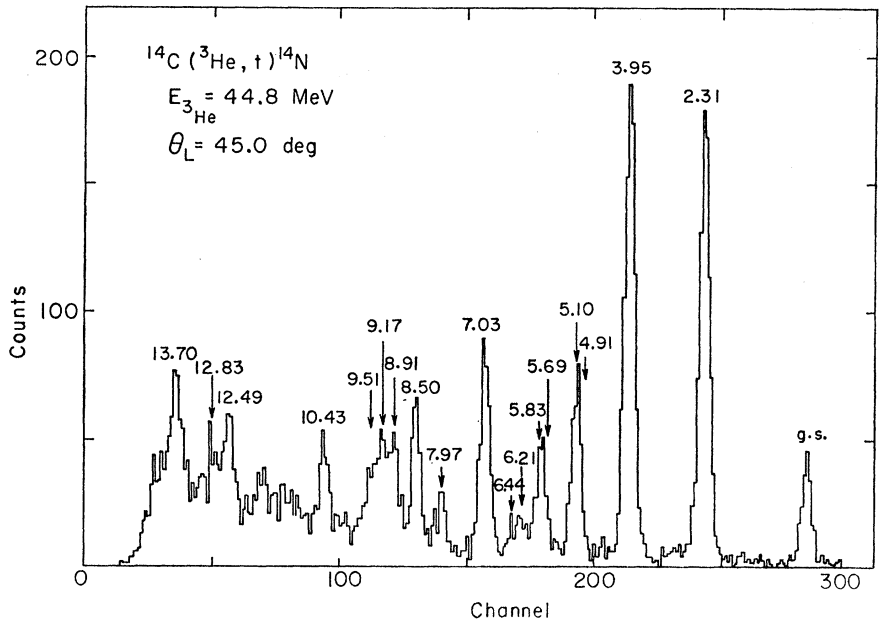

FIG. 4. Energy spectrum of the ^{14}C(^{3}He,t)^{14}N reaction at a ^{3}He energy of 44.8 MeV.

B. Selection Rules

The microscopic formalism which has been described in the previous section implies several restrictions on the various quantum numbers:

$$|J_f - J_i| \leq J \leq J_i + J_f, \tag{14a}$$

$$|j_2 - j_1| \leq J \leq j_1 + j_2, \tag{14b}$$

$$S = 0 \text{ or } 1, \tag{14c}$$

$$|l_2 - l_1| \leq L \leq l_1 + l_2, \tag{14d}$$

$$|L - S| \leq J \leq L + S, \tag{14e}$$

$$|T_f - T_i| \leq T \leq T_f + T_i, \tag{14f}$$

$$|P_i' - P_f'| \leq T \leq 1, \tag{14g}$$

while the conservation of parity gives

$$\pi_f \pi_i = (-)^{l_1 + l_2} = (-)^L. \tag{15}$$

It is interesting to compare the restrictions on the isospin transfer T as they apply to the (^{3}He,t) and (^{3}He,^{3}He′) reactions. First, for a (^{3}He,t) transition, T must be equal to one (14g) and therefore this reaction is only dependent upon the isospin V_{01} and spin-isospin V_{11} terms in the effective interaction, Eq. (4). Second, for a (^{3}He,^{3}He′) reaction where $T_i = T_f = 0$, T must be equal to zero (14f) and only the V_{00} and V_{10} terms contribute to the cross section, whereas if $T_i = T_f \neq 0$, then $T = 0,1$ and all four terms can contribute. Finally, if $T_f = T_i \pm 1$ then only the isospin-dependent terms are allowed (14f,g) for both the (^{3}He,t) and (^{3}He,^{3}He′) reactions.

C. Critical Analysis of Assumptions of Simple Microscopic Description

Several of the simplifying assumptions and possible inadequacies of a simple microscopic description deserve further comment. For example, since the mechanism is assumed to be direct, any contributions from exchange and multiple excitation processes are neglected. It is expected that multiple excitation should be relatively unimportant for levels which have simple shell-model configurations unless some selection rule or accidental cancellation of a nuclear matrix element inhibits the direct process.[8] However, a comparison of the (^{3}He,^{3}He′) and (α,α′) cross sections for transitions restricted to be $S = 1$ indicates that while the contributions from multiple excitation may be small they are not negligible for these transitions (see Sec. IV B2).

Exchange terms result both from antisymmetrization between projectile and target nucleons and from exchange forces in the effective interaction; in general the overlap integrals are complicated and difficult to compute, particularly for complex projectiles. The few calculations which have been reported for nucleon projectiles[30–33] indicate that the contributions from exchange integrals are small for $L = 0$ transitions,[31,33] though for higher L transfers these terms become more important[31–33] and in certain cases the direct and ex-

[30] C. A. Levinson and M. K. Banerjee, Ann. Phys. (N. Y.) **3**, 67 (1958); A. Agodi and G. Schiffrer, Nucl. Phys. **50**, 337 (1964).
[31] T. Une, S. Yamaji and H. Yoshida, Progr. Theoret. Phys. (Kyoto) **35**, 1010 (1966).
[32] K. A. Amos, V. A. Madsen, and I. E. McCarthy, Nucl. Phys. **A94**, 103 (1967).
[33] Jay Atkinson and V. A. Madsen, Lawrence Radiation Laboratory Report No. UCRL-70635, 1967 (unpublished); Bull. Am. Phys. Soc. **13**, 631 (1968).

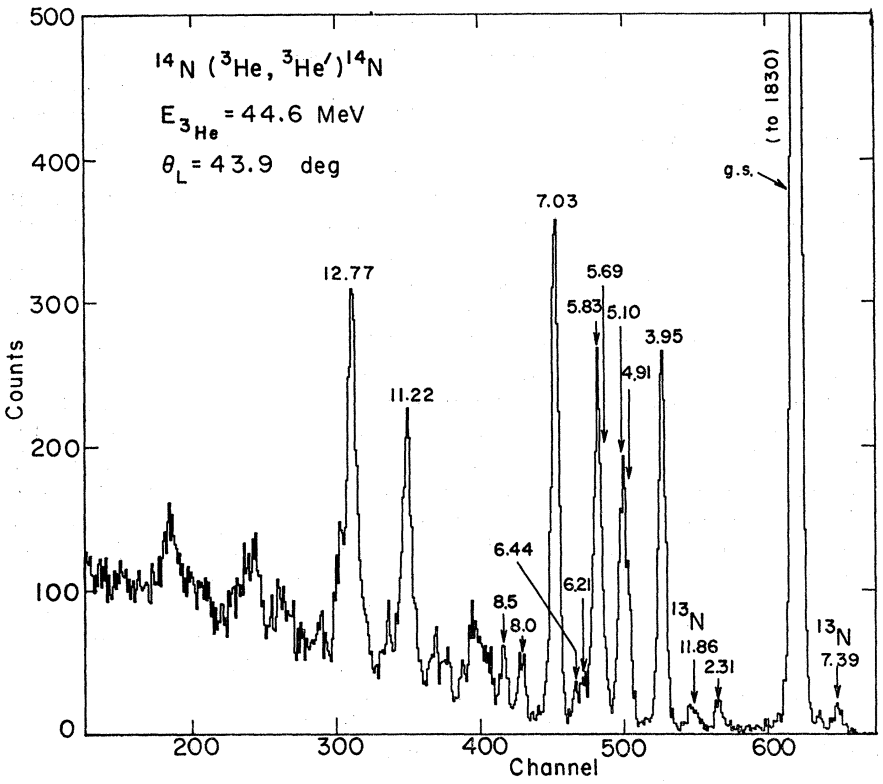

FIG. 5. Energy spectrum of the ^{14}N(^{3}He,^{3}He′)^{14}N reaction at a ^{3}He energy of 44.6 MeV. The peaks corresponding to the 7.39- and 11.86-MeV levels in ^{13}N represent an α contamination in the ^{3}He spectrum.

change contributions can be of comparable magnitude.[32] What the situation would be for the (^{3}He,^{3}He′) and (^{3}He,t) reactions to be considered here is not known. It is evident that more theoretical analyses are necessary before the real importance of exchange effects is fully understood.

Another important approximation concerns the use of a simple local interaction which does not vary with energy and also neglects spin-orbit and tensor forces which are known to contribute to the interaction between free nucleons.[34] The validity of this assumption can only be determined by a comparison with experiment; so far the evidence indicates that this approach can be reasonably successful.[6–12]

Finally, one of the most important criteria for the success of a microscopic description is the reliability of the shell-model wave functions which describe the properties of the initial and final states. Should the wave functions underestimate the observed electromagnetic transition rates ($E2$ and $E3$ especially), then the effective interaction required to fit the corresponding inelastic scattering data would be enhanced. Fortunately, accurate $1p$-shell wave functions are available which have been successful in predicting several nuclear properties including $M1$ transition rates and Gamow-Teller β decays.[19] Furthermore, the effective charges required to predict the observed $E2$ transition rates enhance the $E2$ matrix elements by factors of only 1.5–2.0.[20] As a result, the contributions from collective or "core polarization" effects[8,9] should be smaller for these transitions than those observed for heavier nuclei.

III. EXPERIMENT

The (^{3}He,t) and (^{3}He,^{3}He′) reactions on ^{12}C, ^{13}C, ^{14}C [(^{3}He,t) reactions only], ^{14}N, and ^{15}N were simultaneously investigated using 40–50 MeV ^{3}He beams from the Berkeley 88-in. cyclotron. Particles were detected using two $(dE/dx)-E$ counter telescopes which fed Goulding-Landis particle identifiers[35]; in general, almost complete separation was obtained between tritons and deuterons. The (dE/dx) counters consisted of 8.5-mil (212-μ) or 11.8-mil (295-μ) phosphorus-diffused silicon detectors, while the E counters were 120-mil (3-mm) lithium-drifted silicon detectors. In some experiments it was necessary to rotate the E detectors to an angle of 30° in order to stop the high-energy tritons. Detailed discussions of the experimental equipment have been presented elsewhere.[36–38]

[34] J. L. Gammel, R. S. Christian, and R. M. Thaler, Phys. Rev. **105**, 311 (1957); J. L. Gammel and R. M. Thaler, *ibid.* **107**, 291 (1957); **107**, 1337 (1957); P. S. Signel and R. E. Marshak, *ibid.* **109**, 1229 (1958); E. K. Lassila, M. H. Hull, H. M. Ruppel, F. A. McDonald, and G. Breit, *ibid.* **126**, 881 (1962); T. Hamada and I. D. Johnston, Nucl. Phys. **34**, 382 (1962).

[35] F. S. Goulding, D. A. Landis, J. Cerny, and R. H. Pehl, Nucl. Instr. Methods **31**, 1 (1964).

[36] D. G. Fleming, J. Cerny, C. C. Maples, and N. K. Glendenning, Phys. Rev. **166**, 1012 (1968).

[37] G. W. Butler, J. Cerny, S. W. Cosper, and R. L. McGrath, Phys. Rev. **166**, 1096 (1968).

[38] G. C. Ball, Ph.D. thesis; Lawrence Radiation Laboratory Report No. UCRL-18263, 1968 (unpublished).

A 3.0-in.-diam gas cell with a window of Havar foil 0.1 mil thick[39] was used to contain isotopically pure (>98%) ^{15}N, ^{14}N, and 93% pure ^{13}C in the form of methane. In addition, solid ^{12}C, ^{14}C, and adenine ($C_5H_5N_5$) targets were used.

The ^{14}C target, obtained from Brookhaven National Laboratory, was prepared by depositing ^{14}C onto a 2 mg/cm^2 gold backing. This target contained large amounts of ^{12}C and ^{16}O and the exact ^{14}C target thickness was unknown. In order to obtain absolute cross sections, the $^{14}C(^3He,\alpha)^{13}C$(g.s.) and $^{13}C(\alpha,^3He)^{14}C$(g.s.) reactions were investigated at $E_{^3He}=44.8$ and $E_\alpha=64.5$ MeV, respectively. At these energies, the momentum of the incoming ^3He (outgoing α) particle from the ($^3He,\alpha$) reaction is the same as the momentum of the outgoing ^3He (incoming α) particle from the ($\alpha,^3He$) reaction and therefore time-reversal invariance implies a detailed balance between these two nuclear reactions. Since the cross section for the ($\alpha,^3He$) reaction was accurately measured, it was possible to determine the cross section for the ($^3He,\alpha$) reaction to $\pm 15\%$; the results are discussed in detail elsewhere.[38,40]

Energy spectra for the $^{12}C(^3He,t)^{12}N$, $^{12}C(^3He,^3He')^{12}C$, $^{13}C(^3He,t)^{13}N$, $^{13}C(^3He,^3He')^{13}C$, $^{14}C(^3He,t)^{14}N$, $^{14}N(^3He,^3He')^{14}N$, $^{15}N(^3He,t)^{15}O$, and $^{15}N(^3He,^3He')^{15}N$ reactions are shown in Figs. 1–6; the experimental data for the $^{14}N(^3He,t)^{14}O$ reaction have been published previously in Ref. 18. Typical energy resolutions, full width at half-maximum (FWHM), for tritons and ^3He particles were 150 or 190 keV and 175 or 210 keV, respectively, depending upon whether a solid or gas target was used.

A summary of the levels observed in these experiments and a comparison with previous data[40–56] are presented in Tables I–V. In general, angular distributions between 15° and 80° in the c.m. system were obtained for all prominent levels and are shown in Ref. 38; theoretical distributions for well-known transitions are compared with experiment in Sec. IV B.

IV. MICROSCOPIC DESCRIPTION OF ($^3He,t$) AND ($^3He,^3He'$) REACTIONS

A. Calculation

The theoretical calculations described in this work were carried out using a slightly modified version of the program DRC which has been described elsewhere.[57] This program calculates the quantity $\sigma(j_1j_2L\theta)$ which was defined in Eq. (12). Before a meaningful comparison with experiment could be made, it was necessary to investigate the effects of various parameters and approximations on the shapes and relative magnitudes of the predicted angular distributions. In particular, optical-model parameters, nuclear structure factors, binding energies and bound-state wave functions, range effects and nonlocal potentials will now be discussed in detail.

1. Optical-Model Parameters

The optical-model parameters used in generating the distorted waves were obtained by fitting[58] the ^3He elastic scattering data which was also measured in these experiments. Optical-model parameters for tritons were assumed to be the same as those for ^3He particles. The general form of the optical potential was taken to be

$$U(r)=U_c(r)-V_0(1+e^x)^{-1}-iW_0(1+e^{x'})^{-1}, \quad (16)$$

where

$$x=(r-r_0A^{1/3})/a, \quad x'=(r-r_0A^{1/3})/b,$$

and U_c is the Coulomb potential between a light particle of point-charge and a uniformly charged sphere.

The parameters obtained in this analysis are summarized in Table VI; typical fits are shown in Fig. 7. [Also shown is a fit to the elastic scattering of 40.5-MeV α particles from ^{14}N using the potential set M (see Table VI); this potential set was used in DWBA calculations for inelastic (α,α') transitions (see Sec. IV C1).] With the exception of ^{12}C (the difficulty in fitting

[39] Hamilton Watch Co., Metals Division, Lancaster, Pa.
[40] G. C. Ball and J. Cerny, Bull. Am. Phys. Soc. **12**, 1144 (1967); G. C. Ball and J. Cerny, (unpublished).
[41] C. D. Zafiratos, F. Ajzenberg-Selove, and F. S. Dietrich, Nucl. Phys. **77**, 81 (1966).
[42] F. Ajzenberg-Selove and T. Lauritsen, Nucl. Phys. **A114**, 1 (1968).
[43] F. Ajzenberg-Selove and T. Lauritsen, Nucl. Phys. **11**, 1 (1959).
[44] T. Lauritsen and F. Ajzenberg-Selove, in *Nuclear Data Sheets*, compiled by K. Way *et al.* (Printing and Publishing Office, National Academy of Sciences—National Research Council, Washington 25, D. C., 1962), sets 5 and 6; F. Ajzenberg-Selove (private communication).
[45] R. E. Segel, S. S. Hanna, and R. G. Allas, Phys. Rev. **139**, B818 (1965).
[46] I. Talmi and I. Unna, Phys. Rev. Letters **4**, 469 (1960); N. Vinh-Mau and G. E. Brown, Nucl. Phys. **29**, 89 (1962); D. E. Alburger and D. H. Wilkinson, Phys. Rev. **153**, 1061 (1967).
[47] D. Bachelier, M. Bernas, I. Brissaud, P. Radvanyi, and M. Roy, Nucl. Phys. **88**, 307 (1966); R. L. Kozub, L. A. Kull, and E. Kashy, *ibid.* **A99**, 540 (1967); F. Hinterberger, G. Mairle, V. Schmidt-Rohr, P. Turek, and G. J. Wagner, *ibid.* **A106**, 161 (1968).
[48] G. C. Ball and J. Cerny, Phys. Letters **21**, 551 (1966).
[49] F. C. Barker, Nucl. Phys. **28**, 96 (1961); T. Sebe, Progr. Theoret. Phys. (Kyoto) **30**, 290 (1963).
[50] E. K. Warburton and W. T. Pinkston, Phys. Rev. **118**, 733 (1960); H. J. Rose, Nucl. Phys. **19**, 113 (1960); H. J. Rose, F. Riess, and W. Trost, *ibid.* **52**, 481 (1964).
[51] W. W. True, Phys. Rev. **130**, 1530 (1963).
[52] G. W. Phillips, F. C. Young, and J. B. Marion, Phys. Rev. **159**, 891 (1967) and references given there.
[53] M. Lambert and M. Durand, Phys. Letters **24B**, 287 (1967); R. D. Gill, J. S. Lopes, B. C. Robertson, R. A. I. Bell, and H. J. Rose, Nucl. Phys. **A106**, 678 (1968).
[54] E. K. Warburton, P. D. Parker, and P. F. Donovan, Phys. Letters **19**, 397 (1965); C. R. Gruhn and E. Kashy, Bull. Am. Phys. Soc. **11**, 471 (1966).
[55] E. C. Halbert and J. B. French, Phys. Rev. **105**, 1563 (1957).
[56] B. G. Harvey, J. R. Meriwether, J. Mahoney, A. Bussière de Nercy, and D. J. Horen, Phys. Rev. **146**, 712 (1966).
[57] W. R. Gibbs, V. A. Madsen, J. A. Miller, W. Tobocman, E. C. Cox, and L. Mowry, National Aeronautics and Space Administration Technical Note, NASA TN D-2170, 1964 (unpublished).
[58] A modified version of the computer program SEEK [M. A. Melkanoff, J. Raynal, and T. Sawada, SEEK, Department of Physics, University of California, Los Angeles, Report No. 66-10 (unpublished)] was used in this analysis.

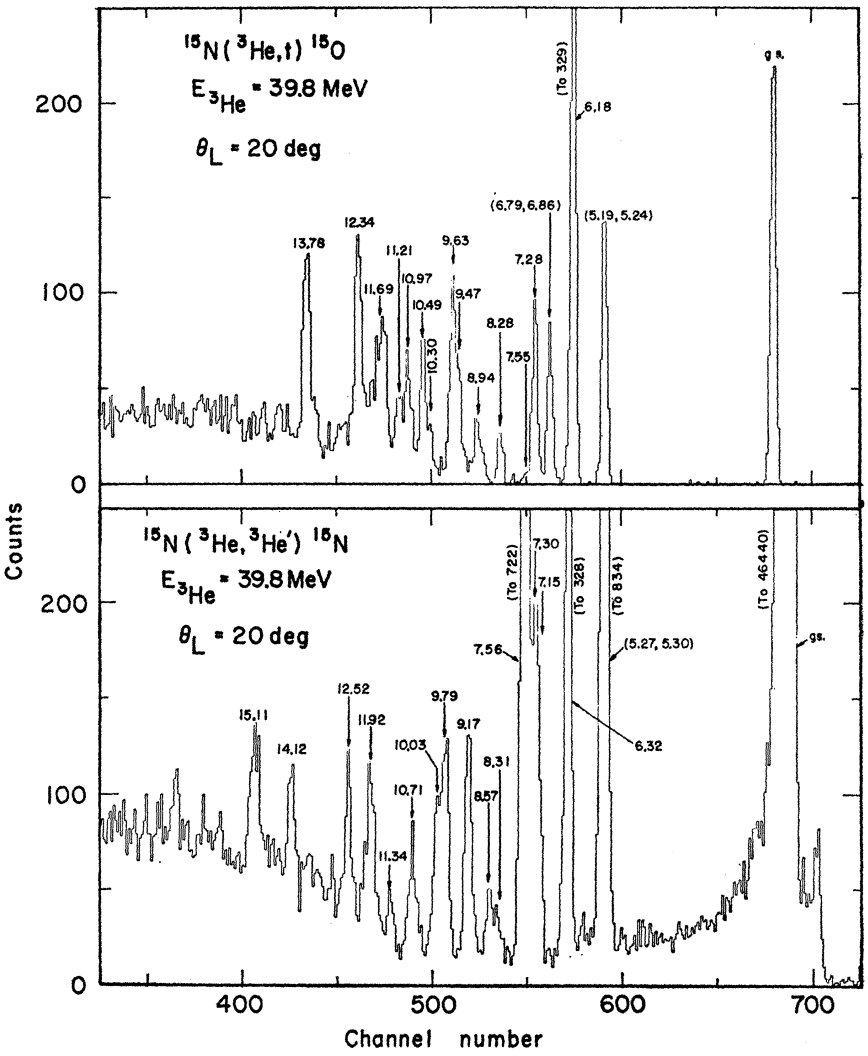

FIG. 6. Energy spectra of the ^{15}N(^{3}He,t)^{15}O and ^{15}N(^{3}He,^{3}He′)^{15}N reactions at a ^{3}He energy of 39.8 MeV. The ^{15}O spectrum has been adjusted to align the mirror levels populated in both reactions.

elastic scattering data from this nucleus is well known[59–61] and will be discussed later), the sets of parameters obtained for each nucleus are almost identical and resemble the ^{3}He potentials for scattering from heavier nuclei.[62]

Unfortunately, when these parameters were used in the DWBA calculations they were unable to give reasonable fits for those (^{3}He,t) $p_{1/2}$, $p_{3/2} \rightarrow p_{1/2}$ transitions in which the total angular momentum transfer was zero. Specifically, these calculations were unable to reproduce the strong minima observed near $\theta_{c.m.} \cong 35°$–45° for dominant $L=0$ transitions with small negative Q values. Identical results were obtained for several parameter sets in the same family possessing real well depths which varied from 160 to 200 MeV. Further investigation showed, however, that the predicted shape of these $L=0$ transitions was very sensitive to small changes in the real radius, and good fits could be obtained if this parameter was decreased by $\approx 7\%$. The ^{3}He(t) optical-model parameters shown in Table VI, modified by setting $r_0' = 0.93 r_0$, were used in calculating the theoretical angular distributions for all transitions observed in the $A = 13$–15 nuclei. Furthermore, since the energy dependence of the optical potentials for ^{3}He particles is known to be weak,[62] these parameters were assumed to be independent of the excitation energy of the final state.

Theoretical angular distributions are shown in Fig. 8 for several shell-model transitions which illustrate that a small decrease in r_0 does not strongly affect the magnitude of these transitions (i.e., the integrated cross sections differ by $<10\%$). Further, with the exception of the $p_{1/2} \rightarrow p_{1/2}$, $L=0$ and $p_{1/2} \rightarrow d_{5/2}$, $L=1 (S=1)$ transitions it has little effect on the predicted shapes of these angular distributions. However, the deep mini-

[59] G. R. Satchler, Nucl. Phys. **A100**, 497 (1967).
[60] E. B. Carter, G. E. Mitchell, and R. H. Davis, Phys. Rev. **133**, B1421 (1964); E. M. Kellogg and R. W. Zurmühle, *ibid.* **152**, 890 (1966).
[61] D. J. Baugh, G. J. B. Pyle, P. M. Rolph, and S. M. Scarrott, Nucl. Phys. **A95**, 115 (1967).
[62] E. F. Gibson, B. W. Ridley, J. J. Kraushaar, M. E. Rickey, and R. H. Bassel, Phys. Rev. **155**, 1194 (1967).

TABLE V. Energy levels observed in ^{15}N and ^{15}O.

^{15}N(^{3}He,^{3}He')^{15}N (Present work) Energy (MeV±keV)	Previous data[a] Energy[b] (MeV±keV)	J^π	^{15}N(^{3}He,t)^{15}O (Present work) Energy (MeV±keV)	Previous data[a] Energy[b] (MeV±keV)	J^π	Dominant shell-model configuration[c]
0.0	0.0	$\frac{1}{2}-$	0.0	0.0	$\frac{1}{2}-$	$p_{1/2}^{-1}$
5.28±30	5.27	$\frac{5}{2}+$	5.24±30	5.24	$\frac{5}{2}(+)$	$(p_{1/2})_0^2 d_{5/2}$
	5.30	$\frac{1}{2}+$		5.19	$\frac{1}{2}+$	$(p_{1/2})_0^2 s_{1/2}$
6.32	6.32	$\frac{3}{2}-$	6.18	6.18	$\frac{3}{2}(-)$	$p_{3/2}^{-1}$
7.15	7.15	$\frac{5}{2}+$	6.84±40	6.86	$\frac{5}{2}+$	$(p_{1/2})_1^2 d_{5/2}$
7.30	7.30	$\frac{3}{2}+$		6.79	$\frac{3}{2}+$	$(p_{1/2})_1^2 s_{1/2}$
7.56	7.56	$\frac{7}{2}+$	7.28	7.28	$\frac{7}{2}(+)$	$(p_{1/2})_1^2 d_{5/2}$
8.31	8.31	$\frac{1}{2}+, (\frac{3}{2}+)$	7.55	7.55	$\frac{1}{2}+$	$(p_{1/2})_1^2 s_{1/2}$
8.57	8.57	$\frac{3}{2}+$	8.28	8.28	$\frac{3}{2}+$	$(p_{1/2})_1^2 d_{5/2}$
9.17±30	9.05	$\frac{1}{2}+, (\frac{3}{2}+)$	8.94±40	8.75	$\frac{1}{2}+$	
	9.16	$\frac{3}{2}(-), (\frac{5}{2})$		8.92	$\frac{3}{2}(+)$	
	9.22	$\frac{3}{2}, (\frac{1}{2})$		8.98	$\frac{3}{2}-$	
9.79±40	9.76	$\frac{5}{2}-$	9.47±50	9.485	$\frac{5}{2}-$	
	9.83	$\frac{7}{2}(-)$		9.49±40	$\frac{3}{2}+$	
10.03±40	9.93	$\frac{1}{2}+, \frac{3}{2}+$	9.63±40	9.61	$\frac{3}{2}-$	
	10.07	$\frac{3}{2}+$		9.67	$(\frac{7}{2}, \frac{9}{2})-$	
	10.45	$\frac{3}{2}, \frac{5}{2}, \frac{7}{2}$	10.30±40	10.28		
	10.54	$\frac{5}{2}$	10.49±40	10.46		
10.71±40	10.70	$\frac{3}{2}+$	10.97±50	10.94	$\geq\frac{3}{2}$	
	10.80	$\frac{3}{2}$		11.02		
11.34±40	[d]		11.21±60	[d]		
11.92±40			11.69±40			
12.52±40			12.34±40			
14.12±40			13.78±40			
15.11±40						

[a] See Refs. 43, 44, 52–55.
[b] Energy levels without error bars were well known previously.
[c] See Refs. 52, 54, 55.
[d] Several levels have been reported above 11 MeV in both ^{15}N and ^{15}O (see Refs. 43 and 44).

mum which is now predicted for the $L=0$ transition at $\theta_{c.m.}\cong 35°$ is in good agreement with relevant experimental data.

The changed shapes of the $p_{1/2}\rightarrow d_{5/2}$, $L=1(S=1)$ transitions were not considered to be as important. [Very few examples of pure or dominant $p_{1/2}\rightarrow d_{5/2}$, $L=1(S=1)$ transitions were observed in these data since the final states were either weakly populated or poorly resolved. Poor fits were obtained using either the modified or unmodified optical potentials and these results will be discussed in Sec. IV B.]

a. ^{3}He scattering from ^{12}C. Difficulties in fitting elastic proton[59] and ^{3}He[61] scattering data for ^{12}C have been reported elsewhere. In this analysis the major difference between the optical-model parameters obtained for ^{12}C and those obtained for other p-shell nuclei is the large imaginary depth W_0 which was required in order to give the best fit (potential set E) to the elastic scattering data (see Table VI). Although there is known to be a strong coupling between the ground and the first excited 2+ state of ^{12}C, an analysis using coupled equations for the scattering of 46-MeV protons from

TABLE VI. Optical-model potentials.

Potential	Channel	Energy (MeV)	V_0 (MeV)	r_0 (F)	a (F)	W_0 (MeV)	r_0 (F)	b (F)	r_c (F)
A[a]	^{15}N+^{3}He	39.8	160.0	1.23	0.595	12.44	1.80	0.858	1.3
B[a]	^{14}N+^{3}He	44.6	160.0	1.29	0.565	11.37	1.78	0.811	1.3
C[a]	^{14}C+^{3}He	44.8	160.0	1.31	0.569	12.58	1.82	0.795	1.3
D[a]	^{13}C+^{3}He	39.6	160.0	1.31	0.565	14.86	1.73	0.826	1.3
X[a]	Average set		160.0	1.29	0.574	12.82	1.78	0.822	1.3
E	^{12}C+^{3}He	49.8	160.0	1.40	0.572	20.31	1.70	0.537	1.3
F[b]	^{12}C+^{3}He	49.8	160.0	1.39	0.542	12.58	1.96	0.571	1.3
M	^{14}N+α[c]	40.5	195.0	1.28	0.654	21.00	1.28	0.654	1.3
$V1$[d]	^{12}C+p	46.3	41.5	1.143	0.643	9.7	1.143	0.643	1.2

[a] In order to fit the reaction data these potentials were modified by setting $r_0'=0.93r_0$.
[b] This potential set was used in calculating the theoretical angular distributions for transitions leading to states in ^{12}C and ^{12}N.
[c] Data obtained by Harvey *et al.* (Ref. 56).
[d] Optical potential set obtained from Ref. 59.

^{12}C indicated that the coupling effects produced only minor changes in the observed optical potential.[59] The large difference in W_0 required to fit the ^{3}He scattering data for ^{12}C seems unreasonable, particularly in view of the above evidence.

If W_0 is fixed at 12.58 MeV, the potential set F is obtained. This potential set is similar to those obtained for other nuclei and the fit to the available elastic scattering data is almost as good as the one obtained using the best fit parameter set E (compare Fig. 7). However, the magnitudes of the inelastic angular distributions calculated using potential sets E and F are very different since the strengths of the imaginary potentials differ by almost a factor of 2.

Finally, it was observed that the experimental $L=0$ transitions leading to states in ^{12}C(^{12}N) were best fit using unmodified optical potentials (i.e., no change in r_0). This may be due to the fact that the observed $L=0$ transitions in ^{12}C(^{12}N) have large negative Q values compared with those in the other nuclei. The unmodified potential set F was chosen in calculating the angular distributions which are compared with experiment in Sec. IV B.

b. Average optical potentials. Since the independent optical-model parameters obtained in the present analysis do not vary greatly from one nucleus to another (with the exception of ^{12}C), an average optical potential set could be used for all nuclei to permit a better comparison of the various strengths obtained for

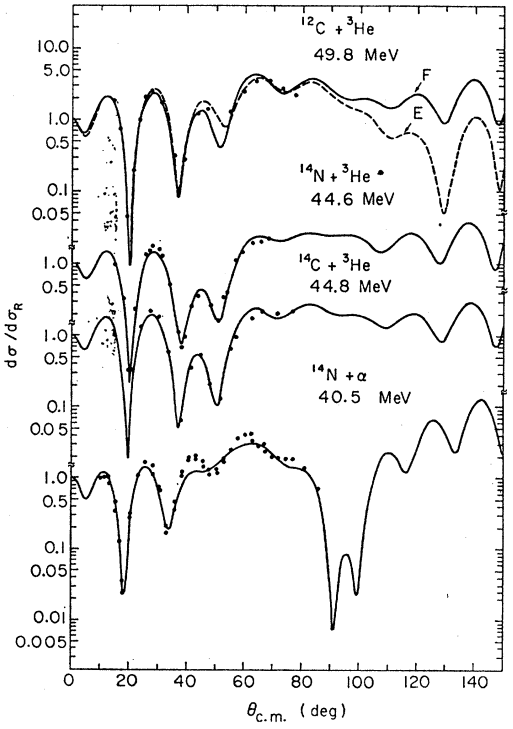

FIG. 7. Typical optical-model fits obtained for the elastic scattering of ^{3}He and α particles from 1p-shell nuclei using the parameters given in Table VI.

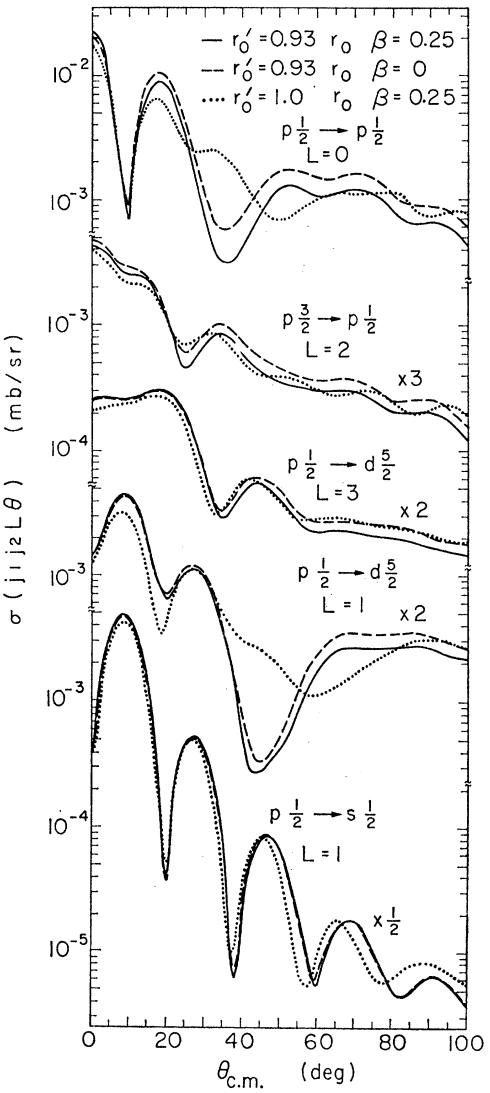

FIG. 8. Single-particle cross sections $\sigma(j_1 j_2 L\theta)$ for typical
$p_{1/2} \rightarrow p_{1/2}$, $L=0$ [^{14}C(^{3}He,t)^{14}N(2.31 MeV, 0+)];
$p_{3/2} \rightarrow p_{1/2}$, $L=2$ [^{14}N(^{3}He,^{3}He′)^{14}N(3.95 MeV, 1+)];
$p_{1/2} \rightarrow d_{5/2}$, $L=3$ [^{15}N(^{3}He,^{3}He′)^{15}N(7.56 MeV, $\frac{7}{2}$+)];
$p_{1/2} \rightarrow d_{5/2}$, $L=1$ [^{14}N(^{3}He,t)^{14}O(6.28 MeV, (3−))];
and
$p_{1/2} \rightarrow s_{1/2}$, $L=1$ [^{13}C(^{3}He,^{3}He′)^{13}C(3.09 MeV, $\frac{1}{2}$+)]
transitions calculated using: (a),(b) modified ($r_0'=0.93r_0$) optical potentials (see Table VI) with a nonlocality range $\beta=0.25$ and $\beta=0$, respectively, and (c) unmodified ($r_0'=r_0$) optical potentials with a nonlocality range $\beta=0.25$.

V_{ST} from fitting different levels in different nuclei. In the present analysis, the inelastic angular distributions that are compared with experiment were computed using the independent optical potential sets. However, the effect of using an average potential set was also investigated as follows: The potential set X was constructed by averaging the values of the parameters for the potential sets A, B, C, and D (compare Table VI). When several representative transitions calculated using

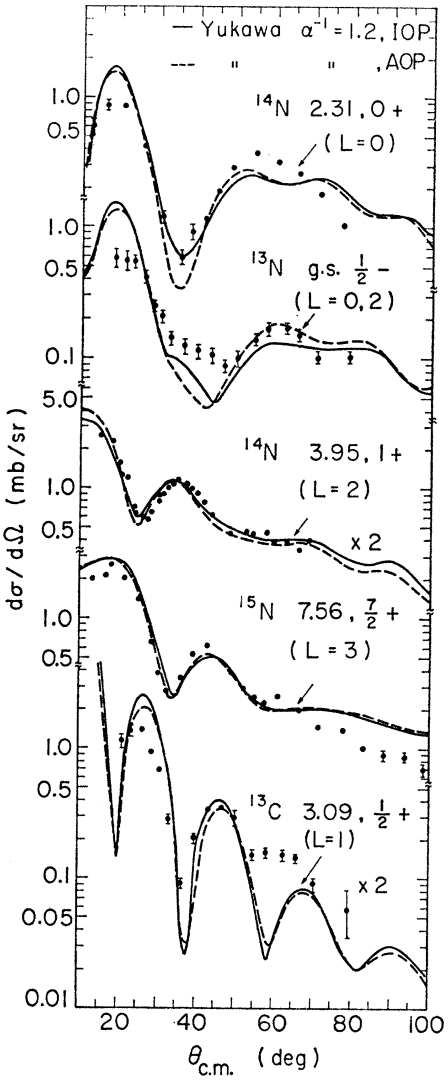

FIG. 9. DWBA predictions for representative (^{3}He,t), [^{14}N 2.31-MeV, 0+; and ^{13}N g.s., ½−] and (^{3}He,^{3}He'), [^{14}N 3.95-MeV, 1+; ^{15}N 7.56-MeV, ½+; and ^{13}C 3.09-MeV, ½+] transitions obtained using the independent optical potentials (IOP) and the average optical potential (AOP) (see Table VI). The curves have been normalized to give the best over-all fit to the experimental data.

this potential set were compared with those predicted using independent optical parameters, it was found that only the magnitudes were affected (compare Fig. 9). In addition, the cross sections for different single-particle transitions were all changed by a similar amount in a given nucleus. As a result it was possible, without actually carrying out a complete additional analysis, to obtain average correction factors which could be applied to all values of V_{ST} obtained earlier from reactions on a given target. These correction factors were 0.87, 0.89, 0.98, 1.19, and 0.98 for ^{12}C, ^{13}C, ^{14}C, ^{14}N, and ^{15}N, respectively. In general it was found[38] that the values of V_{ST} obtained in this manner were in somewhat better relative agreement than those obtained from the independent optical potentials (see also Sec. IV B).

2. *Nuclear Structure Factors*

The nuclear structure factors $G^2(JSLT)$ were computed using the relationships given in Sec. II and are tabulated in Ref. 38. Target-nucleus spectroscopic factors $S(JJ_iJ_f;TT_iT_f;j_1j_2)$ defined in Eq. (A6) of Ref. 5 were calculated for p-shell states using the coefficients of fractional parentage obtained from the wave functions of Cohen and Kurath[21] (hereafter denoted CK); j-j coupling structure factors were also computed for p-shell states to permit comparison with the predictions of CK. [For certain transitions in mass 14, nuclear structure factors were also calculated using the intermediate-coupling wave functions of Visscher and Ferrell (VF).[63]]

Simple shell-model configurations consisting of a $(p_{3/2})^8$ core plus an $s_{1/2}$ or $d_{5/2}$ nucleon for $A=13$ nuclei; a $(p_{1/2},s_{1/2})_{0-,1-;T=0,1}$ or $(p_{1/2},d_{5/2})_{2-,3-;T=0,1}$ configuration for $A=14$ nuclei; and a $[(p_{1/2})_0{}^2, s_{1/2}]_{1/2+;T=1/2,3/2}$, $[(p_{1/2})_0{}^2,d_{5/2}]_{5/2+;T=1/2,3/2}$, $[(p_{1/2})_1{}^2,s_{1/2}]_{1/2+,3/2+;T=1/2}$, or $[(p_{1/2})_1{}^2,d_{5/2}]_{3/2+,5/2+,7/2+;T=1/2}$ configuration for $A=15$ nuclei were assumed for levels which were formed by promoting a p nucleon to the s-d shell. The shell-model calculations of True[51] for levels in ^{14}N and of Halbert and French[55] for levels in ^{15}N and ^{15}O indicate that the above should be reasonably good approximations since these levels only contain small admixtures of other configurations. For example, the wave functions for the $(p_{1/2},s_{1/2})_{1-;T=0,1}$ and $(p_{1/2},d_{5/2})_{2-;T=0,1}$ levels of ^{14}N (see Ref. 51), which have been reasonably successful in predicting γ-ray transition rates,[64,65] only contain $(p_{1/2},d_{3/2})$ admixtures of $\leq 4\%$.

3. *Bound-State Wave Functions, Binding Energies, and Radial Form Factors*

As mentioned previously, in order to simplify the theoretical calculations only one radial form factor $g_L{}^{j_1j_2}(R')$ was computed corresponding to the dominant shell-model transition in the j-j limit [this resulted in Eq. (11)]. Single-particle radial wave functions were calculated using a Woods-Saxon well with a radius of $1.25A^{1/3}$ F, a diffuseness of $a=0.65$ F, and a spin-orbit coupling of 25 times the Thomas term; a Coulomb potential with a radius of $1.25A^{1/3}$ F was also included. The well depths were adjusted to give the binding energies computed from the separation energy scheme illustrated in Fig. 10. If this method is used a definite relationship exists between the binding energies $E_{B1,2}$ of the particle in its initial j_1 and final j_2 states given by $E_{B2}=E_{B1}+Q(p,n)$ for the (^{3}He,t) reaction and $E_{B2}=E_{B1}+Q(p,p')$ for the (^{3}He,^{3}He') reaction.

In order to obtain absolute values for $E_{B1,2}$ it is necessary to determine the parent state in the $(A-1)$ nucleus which has the dominant configuration of the

[63] W. M. Visscher and R. A. Ferrell, Phys. Rev. **107**, 781 (1957).
[64] D. E. Alburger, A. Gallmann, J. B. Nelson, J. T. Sample, and E. K. Warburton, Phys. Rev. **148**, 1050 (1966).
[65] K. P. Lieb and R. Hartmann, Z. Physik **200**, 432 (1967).

inactive $(A-1)$ core of the target nucleus. In general, for $p_{1/2}\rightarrow d_{5/2}$, $p_{1/2}\rightarrow s_{1/2}$, and $p_{1/2}\rightarrow p_{1/2}$ transitions in the j-j limit, the parent state corresponds to the ground state configuration of the $(A-1)$ nucleus and therefore E_{B1} is simply equal to the appropriate nucleon binding energy of the target nucleus. The transitions to levels in ^{15}N(^{15}O) with the configuration $(p_{1/2})_0{}^2d_{5/2}$ or $(p_{1/2})_0{}^2s_{1/2}$ are exceptions to this rule (see Fig. 10). (When this method gave negative values for E_{B2}, the nucleon in its final state was assumed for convenience to be bound by 400 keV.)

For $p_{3/2}\rightarrow p_{1/2}$ transitions, the removal of a $p_{3/2}$ nucleon (in the j-j limit) does not always overlap with the ground-state configuration of the $(A$-1) nucleus but instead may have large coefficients of fractional parentage for several excited states. In this case the radial form factor should in principle be the sum of several radial form factors $g_L{}^{j_1j_2}(R')$, each calculated using bound-state wave functions which were computed for separation energies corresponding to excited states in the $(A-1)$ nucleus. If configuration-mixed wave functions are used for p-shell states, the situation becomes even more complex since $p_{1/2}$, $p_{3/2}\rightarrow p_{3/2}$ transitions also contribute to the population of a given final state. In the present analysis, when several excited states in the $(A-1)$ nucleus were involved in the j-j limit (for $p_{3/2}\rightarrow p_{1/2}$ transitions in mass-13 [(^{3}He,t) reaction only], -14, and -15 nuclei), the binding energy E_{B1} was chosen to be equal to the appropriate nucleon binding energy of the target nucleus plus the excitation energy of the final state in the product nucleus.

The validity of the above for p-shell states depends upon the sensitivity of the predicted angular distributions to changes in the binding energies of the single-particle wave functions. Integrated theoretical cross sections are plotted in Fig. 11 as a function of E_{B1} (the definite relationship between E_{B1} and E_{B2} was maintained) for several different single-particle transitions. In general it was found that both the shapes and the magnitudes of the predicted distributions for $L=0$ and

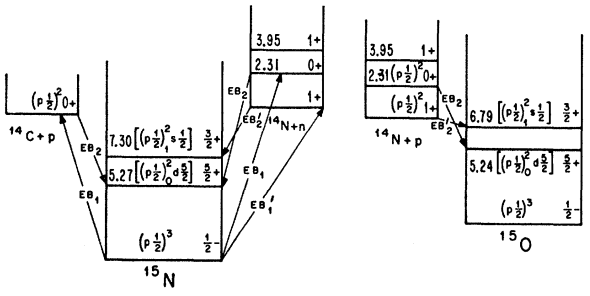

FIG. 10. The separation energy scheme used to determine the binding energies of the target nucleons involved in typical single-particle transitions [i.e., the ^{15}N(^{3}He,^{3}He′)^{15}N(5.27-MeV, $\frac{5}{2}$+) and ^{15}N(^{3}He,t)^{15}O(5.24-MeV, $\frac{5}{2}$+)$p_{1/2}\rightarrow d_{5/2}$; and the ^{15}N(^{3}He,^{3}He′)^{15}N (7.30-MeV, $\frac{3}{2}$+) and ^{15}N(^{3}He,t)^{15}O(6.79-MeV, $\frac{3}{2}$+)$p_{1/2}\rightarrow s_{1/2}$ transitions]. $E_{B1}(E_{B1'})$ represents the binding energy of the $p_{1/2}$ nucleon in its initial j_1 state while $E_{B2}(E_{B2'})$ represents the binding energy of the $d_{5/2}(s_{1/2})$ nucleon in its final j_2 state.

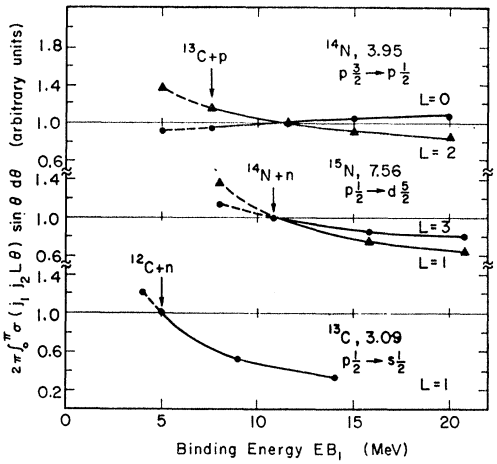

FIG. 11. Integrated single-particle cross sections as a function of the binding energy E_{B1} (the fixed relationship between E_{B1} and E_{B2} was maintained) for several representative single-particle transitions. The cross sections have been normalized relative to those obtained using the binding energies predicted by the separation energy scheme described in Sec. IV A3.

$L=2$ p-shell transitions were relatively insensitive to moderate changes in the binding energy E_{B1}.

One additional assumption was made in calculating the radial form factors for inelastic transitions where the excitation of protons and neutrons both contribute, as is the case for transitions in ^{12}C, ^{14}N, and ^{15}N (the 5.27-MeV, $\frac{5}{2}$+ and 5.30-MeV, $\frac{1}{2}$+ levels only). Since the neutron and proton binding energies are approximately equal for these nuclei, the radial form factors were computed assuming that the bound particles were protons. In ^{14}N, calculations assuming that neutrons were excited gave almost identical angular distributions which differed in magnitude by $<5\%$. (The inelastic transition to the 3.68-MeV, $\frac{3}{2}$− level in ^{13}C also involves both proton and neutron excitations. However, since the neutron and proton binding energies of ^{13}C differ by 12.586 MeV, the theoretical angular distribution for this transition was computed by averaging those calculated assuming that either protons or neutrons were excited.)

4. *Range Effects of Yukawa Interaction*

The theoretical angular distributions for different single-particle transitions and L transfers are shown in Fig. 12 for various ranges of the effective Yukawa interaction between 0.5 and 1.6 F. The predicted differential cross sections have been multiplied by α^6 in order to compare the strengths of different multipole transitions as a function of the range of the interaction [see Eq. (7)]. It can be seen from Fig. 12 that varying the range of the interaction has two general effects on the predicted cross sections. First, the angular distributions have more structure and decrease more rapidly with increasing angle as the range is increased. Second, the strength of the higher multipole transitions is very

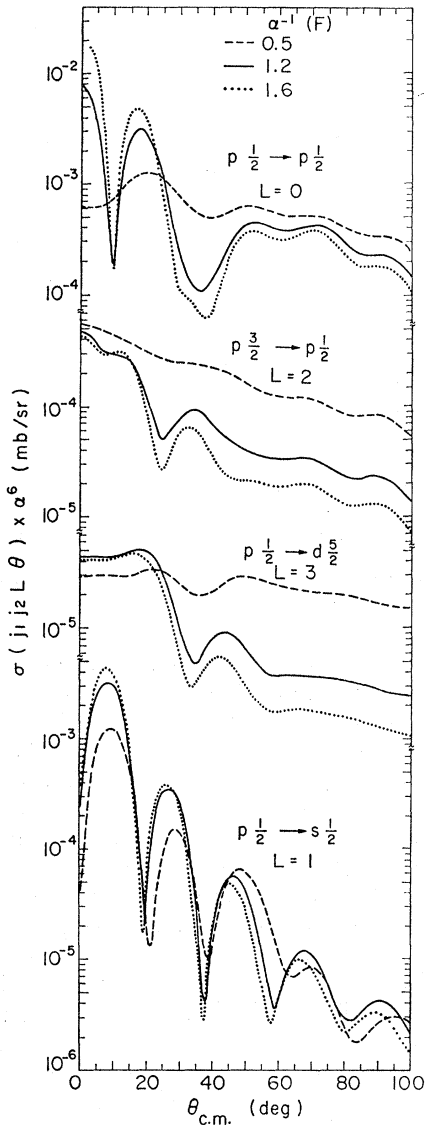

FIG. 12. Single-particle cross sections $\sigma(j_1 j_2 L\theta)$ for typical

$p_{1/2} \rightarrow p_{1/2}$, $L=0$ [^{14}C(^{3}He,t)^{14}N(2.31 MeV, 0+)];
$p_{1/2} \rightarrow p_{3/2}$, $L=2$ [^{14}N(^{3}He,^{3}He′)^{14}N(3.95 MeV, 1+)];
$p_{1/2} \rightarrow d_{5/2}$, $L=3$ [^{15}N(^{3}He,^{3}He′)^{15}N(7.56 MeV, $\frac{7}{2}$+)];
and
$p_{1/2} \rightarrow s_{1/2}$, $L=1$ [^{13}C(^{3}He,^{3}He′)^{13}C(3.09 MeV, $\frac{1}{2}$+)]

transitions calculated using three different ranges of the Yukawa interaction. All cross sections were computed using the independent optical potentials given in Table VI and have been multiplied by α^6 in order to compare the strength of a given single-particle transition (and L transfer) as a function of the range of the interaction.

sensitive to the range of the interaction. For example, in Fig. 12, the strength (i.e., adjusted integrated cross section) of the ^{14}N, 2.31-MeV ($L=0$) transition varies by $\pm 10\%$ between $\alpha^{-1}=0.5$ and 1.6 F while the strength of the ^{14}N, 3.95-MeV ($L=2$) transition decreases by a factor of 5. Similar effects were also observed in an analysis of the ^{90}Zr(p,p')^{90}Zr reaction.[7]

A range of $\alpha^{-1}=1.2$ F was finally chosen for the effective *projectile-nucleon* interaction since it gave the best over-all fit to the experimental angular distributions observed for all L transfers. In order to compare the values of V_{ST} which were measured in these experiments with those obtained from analyses of the (p,p') and (p,n) reactions at $\alpha^{-1}=1.0$ F, it is first necessary to convert the values of $\bar{V}_{ST}$ from an effective *projectile-nucleon* to an effective *nucleon-nucleon* interaction using Eq. (8). Equation (7) must then be used to convert from a range of 1.2 to 1.0 F. The total conversion factors obtained for the (^{3}He,t) and (^{3}He,^{3}He′) reactions were 1.18 and 1.10, respectively; all values quoted in this work have been converted in this manner.

5. *Nonlocal Corrections*

Since the optical-model and shell-model potential wells are known to be nonlocal, the wave functions calculated using an equivalent local potential should actually be reduced inside the nuclear surface.[66] This reduction can be produced using a damping factor obtained from the local energy approximation,[67]

$$G(r)=C[1-(\mu\beta^2/2\hbar^2)U(r)]^{-1/2}, \qquad (17)$$

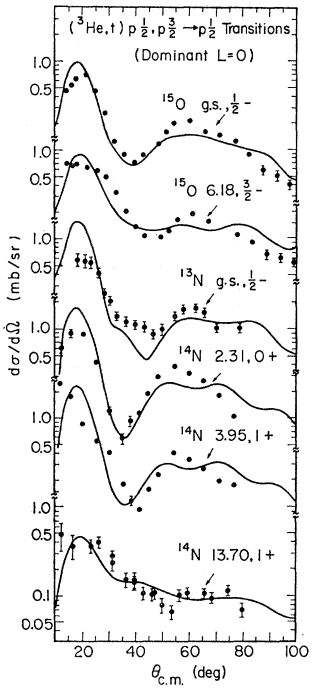

FIG. 13. Angular distributions for (^{3}He,t) $p_{1/2}$, $p_{3/2} \rightarrow p_{1/2}$ (dominant $L=0$) transitions. The solid curves are DWBA predictions obtained using CK wave functions and the independent optical potentials given in Table VI.

[66] F. G. Perey, in *Proceedings of the Conference on Direct Interactions and Nuclear Reaction Mechanisms, Padua, 1962*, edited by E. Clementei and C. Villi (Gordon and Breach Science Publishers, Inc., New York, 1963) p. 125; N. Austern, Phys. Rev. **137**, B752 (1965).

[67] F. G. Perey and D. S. Saxon, Phys. Letters **10**, 107 (1964).

where μ is the reduced mass of the particle, β is the nonlocality range, $U(r)$ is the equivalent local potential, and C is unity for scattering wave functions.

A nonlocal correction was included in this analysis for the ^{3}He and triton optical potentials only, using a nonlocality range of $\beta=0.25$ F.[68] From Fig. 8 it can be seen that the nonlocal damping factor has very little effect on the shapes of the angular distributions but reduces the integrated cross sections for various single-particle transitions by 10–22% with the exception of the $p_{1/2}\rightarrow s_{1/2}$ transition which is reduced by only 1%.

B. Comparison with Experiment

In order to simplify the comparisons with experiment, the transitions observed in the (^{3}He,t) and (^{3}He,^{3}He′) reactions will be discussed in groups according to the particular single-particle transition involved. Furthermore, transitions which deviate strongly from average behavior or transitions which give new spectroscopic information are discussed individually at the end of each section.

As mentioned previously, the theoretical curves which are compared with experiment were all calculated using independent optical potentials; however, strengths were obtained for both independent optical potentials and an average optical potential using the correction factors given in Sec. IV A1. The values quoted in this report will refer to those obtained from the average optical potential unless otherwise stated. In all cases, the theoretical curves were normalized to give the best over-all fit to the experimental data; hence, independent values of V_{ST} were obtained for each transition. When two levels were unresolved experimentally, the theoretical angular distributions were computed by summing the contributions from each transition.

Since more than one term in the effective interaction usually contributed to the cross section of an individual transition, it was necessary to assume some relationship among the relative strengths of the individual terms in the effective interaction. Three different exchange mixtures—including the Wigner interaction (V_{00} only) and the Serber force—were used for (^{3}He,^{3}He′) transitions, while V_{01} and V_{11} were generally assumed to be equal in the analysis of the (^{3}He,t) reaction; this will be discussed further later.

1. (^{3}He,t) $p_{1/2}$, $p_{3/2}\rightarrow p_{1/2}$ *Dominant* $L=0$ *Transitions*

Since the strengths of the higher multipole transitions decrease rapidly with increasing range (see Fig. 12), the ratio of the theoretical cross sections $\sigma(j_1j_2L\theta)$ for $L=0$ to $L=2$ transitions is $\cong 12/1$ at a range of $\alpha^{-1}=1.2$ F. As a result, most (^{3}He,t) transitions which are allowed by the selection rules to be $L=0$ and/or 2 are predicted to be dominant $L=0$ transitions. Transitions to the ground state and the $(p_{3/2},p_{1/2})_{1+,T=1}$ levels in ^{14}O and the 1+ ground state of ^{14}N are the only exceptions to this rule; these levels all have $L=0$ structure factors which are quite small.

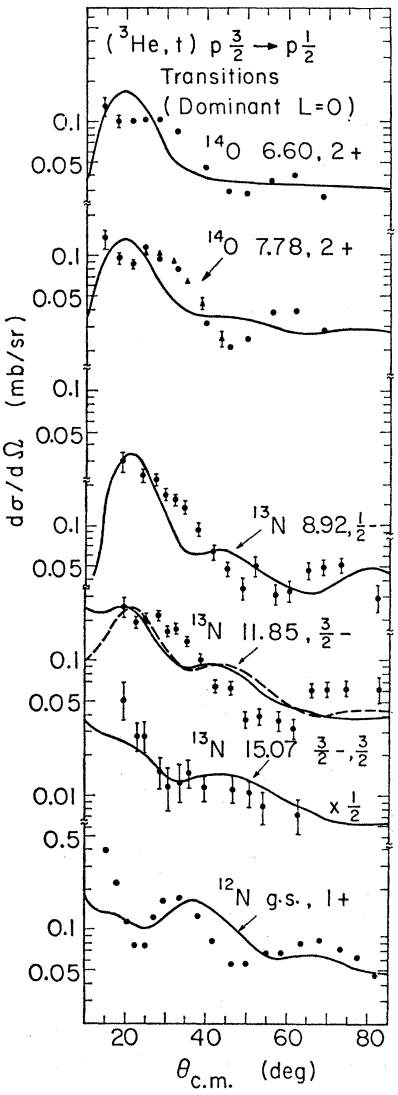

FIG. 14. Angular distributions for (^{3}He,t) $p_{3/2}\rightarrow p_{1/2}$ (dominant $L=0$) transitions. The solid curves are DWBA predictions obtained using CK wave functions and the independent optical potentials given in Table VI. The dashed curve shown for the 11.85-MeV level in ^{13}N was calculated using j-j wave functions.

Theoretical angular distributions for these dominant $L=0$ transitions are compared with experiment in Figs. 13 and 14; the solid curves were calculated using the mixed CK wave functions. In general the fits to these angular distributions are reasonably good, particularly for those levels which have small negative Q values.

Dominant $L=0$ transitions should provide the most accurate determination of the isospin V_{01} and spin-isospin V_{11} terms in the effective interaction. There are

[68] R. H. Bassel, Phys. Rev. 149, 791 (1966); R. Stock, R. Bock, P. David, H. H. Duhm, and T. Tamura, Nucl. Phys. A104, 136 (1967); R. H. Bassel (unpublished).

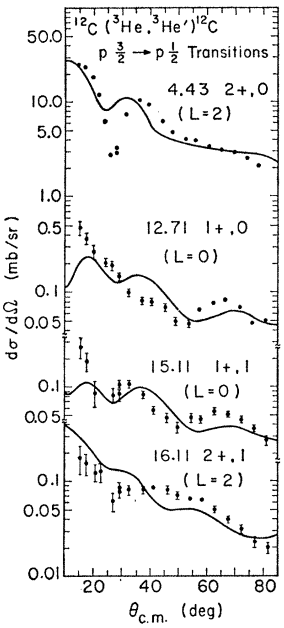

FIG. 15. Angular distributions for $p_{3/2} \rightarrow p_{1/2}$ transitions observed in the ^{12}C(^{3}He,^{3}He′)^{12}C reaction. The solid curves are DWBA predictions obtained using CK wave functions, a Serber exchange mixture, and the optical potential set F (see Table VI).

two reasons for this: First, many of these transitions—particularly the ground isobaric analog transitions—are very insensitive to configuration mixing. Second, $L=0$ transitions are not expected to be enhanced by collective or core polarization effects.[9] Among the transitions which are observed in these experiments, five have been selected which should provide the best measurement of V_{01} and V_{11}; they are transitions to the g.s., $\frac{1}{2}-$ and 6.18-MeV, $\frac{3}{2}-$ levels in ^{15}O; the 2.31-MeV, 0+ and 3.95-MeV, 1+ levels in ^{14}N; and the g.s., $\frac{1}{2}-$ level in ^{13}N.

Three of these transitions are primarily (or only) dependent upon V_{01} while the other two are primarily (or only) dependent upon V_{11}. A ratio of $V_{11}/V_{01} \cong 0.8$ gave the best over-all agreement for these transitions (compare Table VII). This ratio was often used in subsequent calculations for other transitions and L transfers. However, whenever enhanced strengths were observed for V_{01} and V_{11}, the ratio predicted by the Serber force ($V_{11}/V_{01}=1.0$) was used. Consequently, V_{01} and V_{11} were assumed to be equal for all pure $L=2$ and all $p_{1/2} \rightarrow d_{5/2}$ transitions.

The values obtained for V_{01} and V_{11} from all $L=0$ transitions are summarized in Table VII. The agreement among the above five transitions is reasonably good and leads to average values for V_{01} [20.6±0.4 MeV] and V_{11} [16.5±1.1 MeV] which are in excellent agreement with those obtained from an analysis of (p,n) reactions.[8,10–12] In particular, the (p,n) reactions on several target nuclei including ^{14}C, ^{52}Cr, and ^{90}Zr (see Refs. 8, 11, 12) yield values for V_{01} which range from 19 to 26 MeV and the ratio for the spin-isospin strength is determined to be $\cong 0.6-1.0$.[11,12] An independent measurement from the ^{7}Li$(p,n)^7$Be(431 keV) reaction at 44.7 MeV[10] gave a value of $V_{11}=15$ MeV.

It is also interesting to compare the present results with those obtained previously in analyses predominantly concerned with ground isobaric analog state transitions in (^{3}He,t) reactions on ^{17}O, ^{18}O, ^{27}Al, ^{30}Si, ^{39}K, and ^{48}Ti at $E_{^3\mathrm{He}}=18$–25 MeV.[13,14] Using a Yukawa potential with a range of 1.0 F, values were obtained for $V_{01}=31\pm6$ and $V_{11}=20\pm4$ MeV [corrected to an effective *nucleon-nucleon* interaction at 1.0 F (see Eq. (8))]. These strengths are somewhat larger than those obtained in the present analysis; this may be due to a possible energy dependence of the effective interaction.

The relatively large values of V_{01} and V_{11} which are predicted for transitions to the 8.92-, 11.85-, and 15.07-MeV levels in ^{13}N and to the 13.70 MeV level in ^{14}N

TABLE VII. Experimental strengths for the effective *nucleon-nucleon* interaction at $\alpha^{-1}=1.0$ F obtained from (^{3}He,t) $p_{1/2}$, $p_{3/2} \rightarrow p_{1/2}$ (dominant $L=0$) transitions.

Reaction	Energy (MeV)	J^π, T	Independent optical potentials V_{01} (MeV) (jj)	V_{01} (MeV) (CK)	V_{11} (MeV) (jj)	V_{11} (MeV) (CK)	Average optical potential V_{01} (MeV) (jj)	V_{01} (MeV) (CK)	(VF)	V_{11} (MeV) (jj)	V_{11} (MeV) (CK)	(VF)
^{15}N(^{3}He,t)^{15}O	0.0	$\frac{1}{2}-, \frac{1}{2}$[a]	21.6	21.6	(17.3)[b]	(17.3)[b]	21.2	21.2		(17.0)[b]	(17.0)[b]	
	6.18	$\frac{3}{2}-, \frac{1}{2}$[a]	(22.2)	(22.2)	18.1	18.1	(21.7)	(21.7)		17.7	17.7	
^{14}C(^{3}He,t)^{14}N	2.31	0+, 1[a]	20.4	20.4	···	···	20.0	20.0	20.0	···	···	···
	3.95	1+, 0[a]	···	···	21.0	15.7	···	···	···	20.6	15.4	16.5
	13.70	1+, 1	···		17.8	28.4	···	···		17.4	27.8	
^{14}N(^{3}He,t)^{14}O	6.60	2+, 1[c]	(14.2)	(14.8)	11.3	11.8	(16.9)	(17.6)		13.4	14.0	···
	7.78	2+, 1[c]	(13.8)	(14.4)	11.1	11.4	(16.4)	(17.1)		13.2	13.6	
^{13}C(^{3}He,t)^{13}N	0.0	$\frac{1}{2}-, \frac{1}{2}$[a]	22.6	23.3	(18.1)	(18.7)	20.1	20.7		(16.1)	(16.6)	
	3.51	$\frac{3}{2}-, \frac{1}{2}$ [d]	27.7	20.4	27.7	20.4	24.7	18.2		24.7	18.2	
	3.56	$\frac{5}{2}+, \frac{1}{2}$ [d]										
	8.92	$\frac{1}{2}-, \frac{1}{2}$	···	···	18.2	31.6	···	···		16.2	28.1	
	11.85	$\frac{3}{2}-, \frac{1}{2}$	(22.2)	(44.6)	19.7	44.6	(19.8)	(39.7)		17.5	39.7	
	15.07	$\frac{3}{2}-, \frac{3}{2}$	(21.4)	(31.0)	21.4	31.0	(19.0)	(27.6)		19.0	27.6	
^{12}C(^{3}He,t)^{12}N	0.0	1+, 1	···	···	11.6	28.0	···	···		10.1	24.4	
		Average	21.5±0.8	21.8±1.0	19.6±1.5	16.9±1.2	20.4±0.5	20.6±0.4		19.2±1.5	16.5±1.1	

[a] Only these transitions were included in computing average strengths.
[b] In some cases the calculated angular distributions are relatively insensitive to the values of either V_{01} or V_{11}. In these cases the strengths which are obtained are enclosed in parentheses.
[c] These levels were assumed to have the configuration $[(1/\sqrt{2})(p_{3/2},p_{1/2})^{-1} \pm (1/\sqrt{2})(s,d)]_{2+,T=1}$.
[d] A theoretical fit to these unresolved transitions is given in Ref. 38.

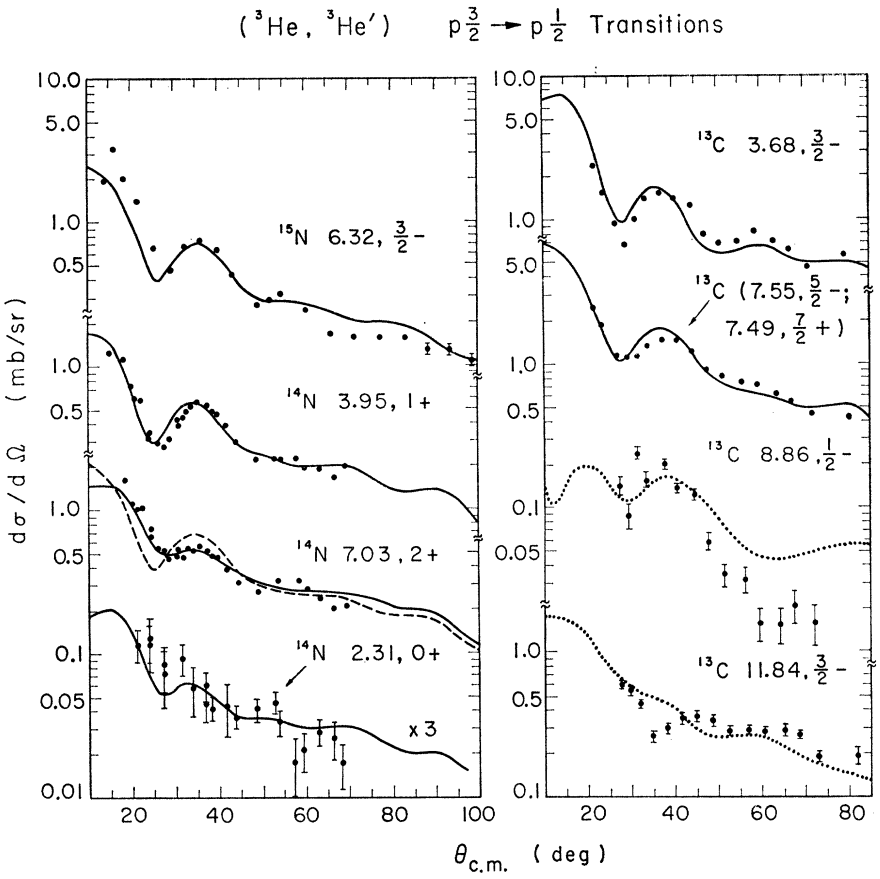

FIG. 16. Angular distributions for (^{3}He,^{3}He′) $p_{3/2} \rightarrow p_{1/2}$ transitions. The solid curves are DWBA predictions obtained using CK wave functions, a Serber exchange mixture, and the independent optical potentials given in Table VI. The dashed curve shown for the 7.03-MeV level in ^{14}N was calculated using a Wigner force. The dotted curves for ^{13}C transitions were computed using the unmodified ($r_0' = r_0$) potential set D (see Table VI); furthermore, force III was used for the 8.86-MeV level of ^{13}C, while a Wigner interaction was assumed for the 11.84-MeV level.

may indicate that the wave functions of CK are unable to account for the configuration mixing in these states. This is particularly true for the 11.85-MeV level in ^{13}N, since it will be shown later that the ^{13}C(^{3}He,^{3}He′)^{13}C reaction, which populates the mirror level in ^{13}C at 11.84 MeV, predicts a value for V_{00} which is several times larger than the values obtained for other transitions. In addition, evidence from an analysis of the ^{15}N(p,t)^{13}N reaction[36] indicates that the wave functions of CK underestimate the cross section for the 8.92-MeV, $\frac{1}{2}-$ level in ^{13}N by a factor of 600.

2. (^{3}He,^{3}He′) $p_{3/2} \rightarrow p_{1/2}$ ($T_f = T_i$) Transitions

In general, the (^{3}He, ^{3}He′) reaction is expected to be relatively insensitive to the spin- and isospin-dependent terms in the effective two-body interaction. This results from the following: (1) The Wigner interaction for complex projectiles is enhanced by a factor equal to the number of nucleons in the incoming projectile, and (2) evidence from nucleon-nucleon (see Sec. IV C3) and nucleon-nucleus[7–9] scattering data indicates that V_{00} is probably two to three times larger than V_{10}, V_{01}, and V_{11}. Consequently, if V_{00} is allowed, the ($JSLT$) = ($L0L0$) amplitudes are predicted to be the dominant terms for all inelastic transitions.

For $p_{3/2} \rightarrow p_{1/2}$ transitions, the ($L0L0$) = (0000) amplitude is generally forbidden by the selection rules, Eqs. (14a), (14b), (14e), and therefore most of these transitions are predicted to have dominant $L=2$ distributions. The experimental angular distributions obtained for $p_{3/2} \rightarrow p_{1/2}$ transitions are shown in Figs. 15 and 16; only those transitions in which $T_f = T_i$ will be discussed in this section. A comparison with those transitions which are restricted to be pure $L=2$ (i.e., the 4.43 MeV, 2+ level in ^{12}C and the 7.55 MeV, $\frac{5}{2}-$ level in ^{13}C) indicates that all $p_{3/2} \rightarrow p_{1/2}$ transitions have a characteristic $L=2$ distribution with the exception of transitions which must be $S=1$, (i.e., the 12.71-MeV, 1+ level in ^{12}C and the 8.86-MeV, $\frac{1}{2}-$ level[69] in ^{13}C).

In order to investigate the sensitivity of these [and other (^{3}He,^{3}He′)] transitions to the spin and isospin dependence of the effective interaction, three different approximations were made concerning the exchange mixture in the central two-body force. First, calculations were carried out assuming that only V_{00} contributes to the experimental cross sections (denoted

[69] A ($JSLT$) = (0000) amplitude is allowed for the 8.86 MeV, $\frac{1}{2}-$ level in ^{13}C if CK wave functions are used. However, nuclear structure factor calculations predict that this amplitude is approximately zero.

TABLE VIII. Experimental strengths for the effective *nucleon-nucleon* interaction at $\alpha^{-1}=1.0$ F obtained from (^{3}He,^{3}He'), $p_{3/2}\rightarrow p_{1/2}$ transitions.

		Energy (MeV)	J^π, T	V_{00} (MeV) Wigner force (jj)	Wigner force (CK)	Serber force (jj)	Serber force (CK)	Force III (jj)	Force III (CK)
A. Independent optical potentials	^{15}N	6.32	$\frac{3}{2}-,\frac{1}{2}$	68.8	68.8	77.3	77.3	49.3	49.3
	^{14}N	3.95	$1+,0$	41.1	41.6	39.5	41.1	39.5	41.1
		7.03	$2+,0$	50.3	53.5	42.8	43.9	42.8	43.9
	^{13}C	3.68	$\frac{3}{2}-,\frac{1}{2}$	82.2	61.1	71.2	58.1	83.4	59.7
		7.55[a]	$\frac{5}{2}-,\frac{1}{2}$	112.6	76.3	126.5	82.0	98.3	71.1
		11.84[b]	$\frac{3}{2}-,\frac{1}{2}$	150.2	2010.	168.4	332.4	77.0	157.8
	^{12}C	4.43	$2+,0$	106.6	67.8	105.8	67.8	105.8	67.8
			Average	76.9±24	61.5±9	77.1±26	61.7±14	69.9±26	55.5±11
B. Average optical potential	^{15}N	6.32	$\frac{3}{2}-,\frac{1}{2}$	67.4	67.4	75.8	75.8	48.3	48.3
	^{14}N	3.95	$1+,0$	48.9	49.5	47.0	49.3	47.0	49.3
		7.03	$2+,0$	59.9	63.7	50.9	52.2	50.9	52.2
	^{13}C	3.68	$\frac{3}{2}-,\frac{1}{2}$	73.2	54.4	63.4	51.7	74.2	53.1
		7.55[a]	$\frac{5}{2}-,\frac{1}{2}$	100.2	67.9	112.6	73.0	87.5	63.3
		11.84[b]	$\frac{3}{2}-,\frac{1}{2}$	133.6	1790.	149.8	296.0	68.5	140.3
	^{12}C	4.43	$2+,0$	92.7	59.0	92.0	59.0	92.0	59.0
			Average	73.7±15	60.3±6	73.6±20	60.2±10	78.1±19	54.2±5

[a] The contribution from the 7.49-MeV, 7/2+ level has been neglected.
[b] Not included in computing average strengths.

Wigner force). Second, a Serber exchange mixture was used; this force predicts relative strengths in the ratio

$$V_{00}:V_{10}:V_{01}:V_{11}=-3:1:1:1.$$

Finally, a recent analysis of the (p,p') reaction[9] indicated that the proton-proton interaction was appreciably stronger than the proton-neutron interaction, implying that V_{00} and V_{01} have the same sign; more tentative results showed that possibly V_{10} and V_{11} have opposite signs.[9] Since the inelastic transitions in mirror nuclei are dependent upon the signs of V_{ST} [i.e., $T=0$ and 1 transfers are both allowed, see Eqs. (14f), (14g)], an empirical exchange mixture denoted force III was also used. This force was assumed to give strengths in the ratio

$$V_{00}:V_{10}:V_{01}:V_{11}=-3:-1:-1:1.$$

This sign convention was chosen to satisfy the normalization condition[4]: $V_{00}+V_{10}-3(V_{01}+V_{11})=-1$.

The solid curves shown in Figs. 15 and 16 for $p_{3/2}\rightarrow p_{1/2}$ (dominant $L=2$) transitions were calculated using mixed CK wave functions and assumed the Serber exchange mixture (the $S=1$ transitions will be discussed later). In general, the shapes of the theoretical distributions calculated using other exchange mixtures were almost identical. In order to obtain independent values of V_{00} for each transition and each exchange mixture, the theoretical curves have been normalized to give the best over-all fit to the experimental data; the results are summarized in Table VIII.

Several conclusions are evident from these results. First, the values obtained for V_{00} are generally insensitive to the particular exchange mixture used, and therefore little information can be obtained from these transitions concerning the spin and isospin dependence of the central interaction. Second, as was anticipated (with the exception of the 11.84-MeV level in ^{13}C which will be discussed later), the relative agreement for all transitions is noticeably improved and the strength required for V_{00} is smaller using the mixed CK wave functions.

One of the most important results, however, is the magnitude of the strength obtained here for V_{00} [60.2±10 MeV] (the values quoted for V_{00} will refer to those obtained using a Serber exchange mixture unless otherwise stated) without core polarization effects. In previous analyses of the (p,p') reaction values for $V_{00}\cong 200$ MeV were obtained (for $\alpha^{-1}=1.0$ F) for inelastic transitions in ^{18}O, ^{52}Cr, ^{54}Fe, ^{90}Zr, and ^{208}Pb when the ground and lower excited states were assumed to be well described by simple shell-model configurations.[8] If core polarization effects were included, however, V_{00} was reduced to approximately 80 MeV.[9] Regarding the present analysis for p-shell transitions, the wave functions of CK are unable to predict the observed $E2$ rates without including effective charges of βe for neutrons and $(1+\beta)e$ for protons where $\beta=0.5$.[20] However, the resulting enhancement factors for $E2$ transition matrix elements only range from 1.5 to 2.0. Therefore, core polarization effects should be less important but not negligible for $1p$-shell transitions.

Without specifically including core polarization in the microscopic analysis, it is difficult to determine how much this effect would alter the present (^{3}He,^{3}He') results; however, the relatively small values which were obtained for V_{00} indicate that core polarization is

TABLE IX. Experimental strengths[a] for the effective *nucleon-nucleon* interaction at $\alpha^{-1}=1.0$ F obtained from (^{3}He,^{3}He′) transitions where V_{00} is forbidden.

Dominant single-particle transition		Energy (MeV)	J^π, T		Serber force (jj)	Serber force (CK)	Force III (jj)	Force III (CK)
$p_{1/2}\rightarrow d_{5/2}$	^{15}N	8.57	$\frac{3}{2}+,\frac{1}{2}$	V_{10}, V_{11}[b]	22.0		...[c]	
$p_{1/2}\rightarrow p_{1/2}$	^{14}N	2.31	$0+,1$	V_{11}	14.7	20.2	14.7	20.2
$p_{3/2}\rightarrow p_{1/2}$	^{13}C	8.86	$\frac{1}{2}-,\frac{1}{2}$	V_{10}, V_{11}	...[c]	294	14.3	26.5
$p_{3/2}\rightarrow p_{1/2}$	^{12}C	12.71	$1+,0$	V_{10}	10.6	27.0	10.6	27.0
$p_{3/2}\rightarrow p_{1/2}$		15.11	$1+,1$	V_{11}	10.2	24.3	10.2	24.3
$p_{3/2}\rightarrow p_{1/2}$		16.11	$2+,1$	V_{01}, V_{11}	29.4	46.1	29.4	46.1

[a] The values given here and in all subsequent tables were obtained using the average optical potential.
[b] $|V_{10}|=|V_{11}|$ for both a Serber exchange mixture and Force III.
[c] Forbidden in the j-j limit.

definitely less important in this treatment of $1p$-shell nuclei. Further evidence from an investigation of the ^{7}Li(p,p')^{7}Li(478 keV) reaction supports this conclusion[10]: At an incident proton energy of 44.7 MeV the strength required to fit the total cross section was $V_{00}=90$ MeV (for a Yukawa with $\alpha^{-1}=1.0$ F). In addition, an analysis of the ^{12}C(p,p')^{12}C (4.43 MeV) reaction at $E_p=46$ MeV[70] (see Sec. IV C2) gave a value of $V_{00}=86.9$ MeV to be compared with $V_{00}=59.0$ MeV obtained from the (^{3}He,^{3}He′) reaction.

a. 11.84-MeV, $\frac{3}{2}-$ level in ^{13}C. The wave functions of CK predict that the ^{13}C(^{3}He,^{3}He′)^{13}C (11.84 MeV, $\frac{3}{2}-$) transition should be very sensitive to the spin- and isospin-dependent terms in the effective interaction [i.e., the (2020) amplitude is predicted to be very small]. However, the strength required for V_{00}[296 MeV] to fit the observed cross section for this transition is several times larger than those obtained for other $p_{3/2}\rightarrow p_{1/2}$ transitions. In addition, evidence from the ^{13}C(α,α')^{13}C reaction at $E_\alpha=64.5$ MeV[71] indicates that the 11.84 level is populated with approximately the same relative intensity as observed in the (^{3}He,^{3}He′) reaction. Since the (α,α') reaction is only dependent upon V_{00}, it is evident that the mixed CK wave functions are definitely unable to account for the population of this state.

b. ^{12}C 12.71-MeV, 1+ and ^{13}C 8.86-MeV, $\frac{1}{2}-$ levels. Since the ^{12}C 12.71-MeV, 1+ and ^{13}C 8.86-MeV, $\frac{1}{2}-$ levels are predicted to be dominant $L=0$, $S=1$ transitions, they provide a direct measure of the V_{10} term in the effective interaction (the 8.86-MeV level also depends upon V_{11}). Unfortunately, both of these levels are populated in the (α,α') reaction[56] with almost the same relative intensity as in the (^{3}He,^{3}He′) reaction. The 12.71-MeV, 1+ level in ^{12}C is an example of the well-known unnatural parity states which have been investigated extensively in the (α,α') reaction.[72,73] In some cases it has been shown that the population of these states can be explained by multiple excitation processes.[73] As a result, the values obtained for V_{10} in the present analysis only provide an upper limit on the magnitude of this term.

The theoretical angular distributions for these transitions are compared with experiment in Figs. 15 and 16. Both transitions are best fit using unmodified optical

TABLE X. Experimental strengths for the effective *nucleon-nucleon* interaction at $\alpha^{-1}=1.0$ F obtained from (^{3}He,t), $p_{3/2}\rightarrow p_{1/2}$ (dominant $L=2$) transitions.

Reaction	Energy (MeV)	J^π, T	V_{01} (MeV) (jj)	V_{01} (MeV) (CK)	V_{01} (MeV) (VF)	V_{11} (MeV) (jj)	V_{11} (MeV) (CK)	V_{11} (MeV) (VF)
^{14}C(^{3}He,t)^{14}N	0.0	$1+,0$	...	...	...	17.7	23.7	25.9
	7.03	$2+,0$[a]	35.5	35.2	34.8	35.5	35.2	34.8
	10.43[b]	$2+,1$[a]	44.9	48.3		44.9	48.3	
^{14}N(^{3}He,t)^{14}O	0.0	$1+,0$	...	...	...	15.1	20.8	23.7
	10.89[c]	$(1+),1$	14.0	17.7		11.2	14.2	
	11.24[c]	$(1+),1$	19.3	24.6		15.5	19.6	
^{13}C(^{3}He,t)^{13}N	7.39	$\frac{5}{2}-,\frac{1}{2}$[a]	33.1	40.3		33.1	40.3	
^{12}C(^{3}He,t)^{12}N	0.96	$2+,1$[a]	29.3	45.8		29.3	45.8	
		Average	35.7±5	42.4±5		35.7±5	42.4±5	

[a] Only these transitions were included in computing average strengths.
[b] The 10.43-MeV level is assumed to have the configuration $[(1/\sqrt{2})(p_{3/2},p_{1/2})^{-1}\pm(1/\sqrt{2})(s,d)]_{2+,T=1}$.
[c] These values for V_{ST} were obtained assuming that either the 10.89 or the 11.24 MeV level had the dominant configuration $(p_{3/2},p_{1/2})^{-1}{}_{1+,T=1}$.

[70] E. L. Petersen, I. Slaus, J. W. Verba, R. F. Carlson, and J. Reginald Richardson, Nucl. Phys. **A102**, 145 (1967).
[71] G. C. Ball and J. Cerny (unpublished).
[72] W. W. Eidson and J. G. Cramer, Jr., Phys. Rev. Letters **9**, 497 (1962).
[73] T. Tamura, Nucl. Phys. **73**, 241 (1965); J. S. Vincent, E. T. Boschitz, and J. R. Priest, Phys. Letters **25B**, 81 (1967).

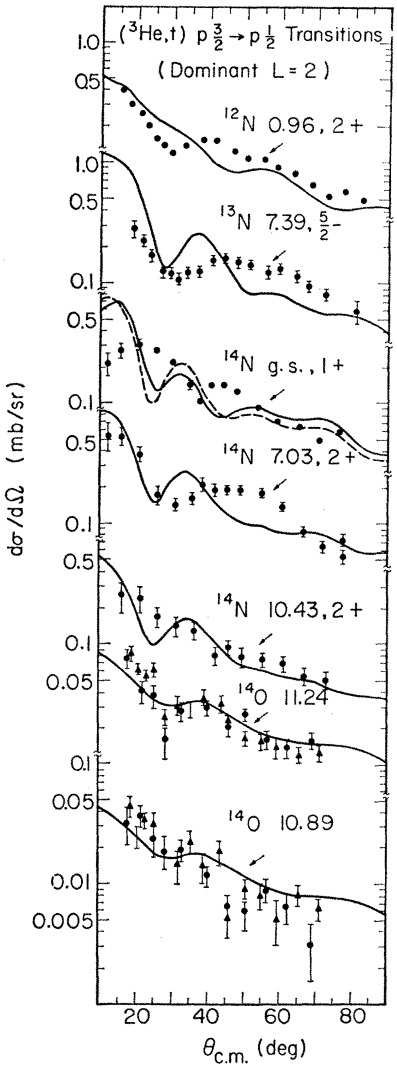

FIG. 17. Angular distributions for the (^{3}He,t) $p_{3/2}\rightarrow p_{1/2}$ dominant $L=2$ transitions. The solid curves are DWBA predictions obtained using CK wave functions and the independent optical potentials given in Table VI. The dashed curve shown for the ground state of ^{14}N was computed using VF wave functions.

potentials; however, the agreement is not as good as that generally obtained for the (^{3}He,t) $L=0$ and (^{3}He,^{3}He′) $L=2$ transitions. The values predicted for V_{10} and V_{11} are shown in Table IX. (Only the values obtained using the average optical potential set will be presented in Table IX and in all subsequent tables; those obtained using independent optical potentials are tabulated in Ref. 38.) If a Serber exchange mixture is used, the ^{13}C(^{3}He,^{3}He′)^{13}C (8.86-MeV, $\frac{1}{2}$−) transition is severely restricted using CK wave functions; however, if force III is used both transitions predict strengths of $V_{10}\approx 27$ MeV using CK wave functions. No conclusive determinations of this term have been obtained from (p,p') data; tentative results give $|V_{10}|\approx 40$ MeV.[9]

3. (^{3}He,t) $p_{3/2}\rightarrow p_{1/2}$ Dominant $L=2$ Transitions

The transitions which are discussed in this section can be divided into two groups: (1) those transitions which are restricted by the selection rules to be pure $L=2$, and (2) those transitions which could be $L=0$ and $L=2$ but whose $L=0$ amplitudes are predicted to be relatively small—transitions to the 0+ ground state and the $(p_{3/2},p_{1/2})_{1+,T=1}$ levels in ^{14}O and the 1+ ground state in ^{14}N. The second group will be discussed later.

The pure $L=2$ (^{3}He,t) transitions all have characteristic angular distributions which are similar to the $L=2$ (^{3}He,^{3}He′) distributions but have much less structure and are not as well reproduced by theoretical calculations (see Fig. 17). The values obtained for V_{01} and V_{11} shown in Table X are consistently higher than those required for $L=0$ transitions. It would be necessary to

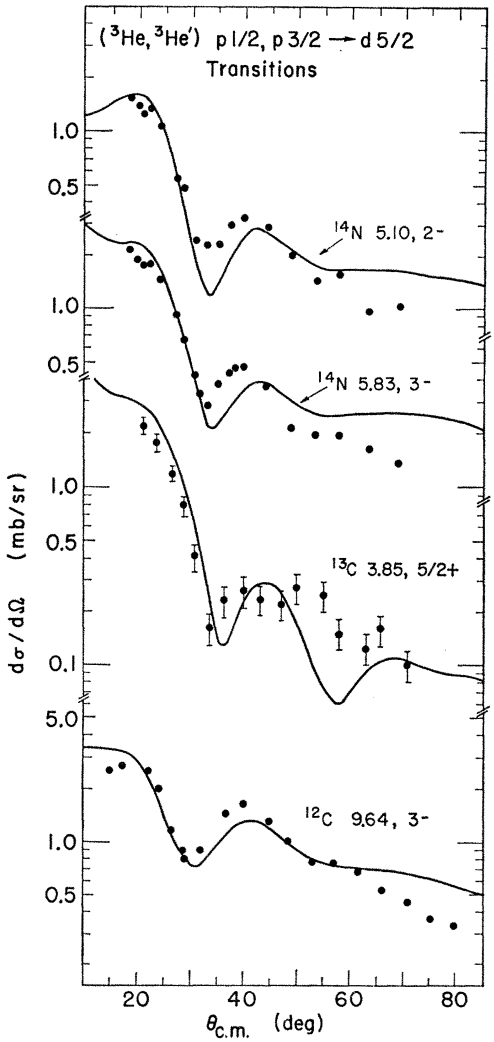

FIG. 18. Angular distributions for (^{3}He,^{3}He′) $p_{1/2}$, $p_{3/2}\rightarrow d_{5/2}$ transitions. The solid curves are DWBA predictions obtained using j-j wave functions, a Serber exchange mixture, and the independent optical potentials given in Table VI. (The 9.64-MeV, 3− level in ^{12}C was assumed to have the configuration $(p_{3/2})_{3/2}{}^7 d_{5/2}$).

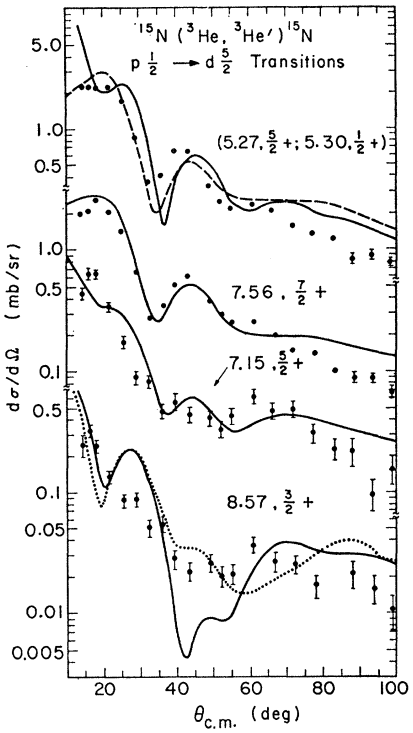

FIG. 19. Angular distributions for $p_{1/2} \rightarrow d_{5/2}$ transitions observed in the $^{15}N(^3He,^3He')^{15}N$ reaction. The solid curves are DWBA predictions obtained using j-j wave functions, a Serber exchange mixture, and the modified optical potential set A (see Table VI). The dashed curve shown for the unresolved levels at 5.27 and 5.30 MeV was computed neglecting the contribution from the 5.30-MeV, $\frac{1}{2}+$ level. The dotted curve shown for the 8.57-MeV, $\frac{3}{2}+$ level was computed using the unmodified potential set A.

use a range of ≈ 0.5 F to obtain agreement between the relative strengths required for the $L=0$ and the $L=2$ transitions; however, the fits obtained at this range would be very poor for all transitions (compare Fig. 12). The apparent enhancement of the (^{3}He,t) $L=2$ transitions may be due to collective or core polarization effects as discussed previously for (^{3}He,^{3}He′) $p_{3/2} \rightarrow p_{1/2}$ transitions. The structureless features of the angular distributions for these transitions might indicate, however, that other mechanisms such as multiple excitation or particle exchange are contributing.

a. $^{14}N(^3He,t)^{14}O(g.s.,0+)$ and $^{14}C(^3He,t)^{14}N(g.s.,1+)$ transitions. The $^{14}N(^3He,t)^{14}O$(g.s.,0+) reaction and the inverse of the $^{14}C(^3He,t)^{14}N$(g.s.,1+) reaction correspond to transitions between identical initial and final states if one assumes the charge independence of nuclear forces. When detailed-balance and phase-space corrections are applied, the angular distributions for these transitions should be identical (see also Sec. V). Evidence from the well-known β decay of ^{14}C predicts that the $L=0$ amplitudes for these transitions are very small.[63] It was experimentally observed—as will be further discussed and illustrated in Sec. V B—that both of these transitions have a distinct angular distribution which is neither pure $L=0$ nor pure $L=2$ in character. The $^{14}C(^3He,t)^{14}N$(g.s.,1+) data are fit in Fig. 17. Theoretical calculations using mixed CK or VF wave functions predict a dominant $L=2$ distribution while those using j-j wave functions additionally include a strong $L=0$ component; none of these permit a good fit to the experimental data. The values obtained for V_{11} are shown in Table X; both the $^{14}N(^3He,t)^{14}O$ (g.s.,0+) and $^{14}C(^3He,t)^{14}N$ (g.s.,1+) transitions predict similar results. Using mixed wave functions one notes that the strengths required are about 40–50% larger than those obtained for $L=0$ transitions.

It is interesting to compare these results with those obtained in a recent microscopic analysis of the $^{14}C(p,n)^{14}N$ reaction at $E_p=13.3$ MeV.[11] When a Yukawa interaction with a range of 1.4 F was used, comparison with experiment showed not only a poor fit to the ground-state transition but also a strength for V_{11} (using mixed VF wave functions) which was three times larger (or ≈ 58 MeV at $\alpha^{-1}=1.0$ F) than the value of 19.2 MeV required to fit the (p,n) transition to the 3.95-MeV level. In contrast, the corresponding values required in the $^{14}C(^3He,t)^{14}N$ reactions are 25.9 and 16.5 MeV, respectively. This discrepancy may indicate that contributions from other reaction mechanisms such as particle exchange are not as important for complex projectiles at higher incident energies.

b. 10.89- and 11.24-MeV levels in ^{14}O. The 10.89- and 11.24-MeV levels in ^{14}O are both candidates for the analog to the 13.70-MeV, $(p_{3/2},p_{1/2})^{-1}{}_{1+,T=1}$ level in ^{14}N which should occur near 11.4 MeV in ^{14}O if level shifts are neglected. The structure factor calculations predict that the angular distribution to this state should correspond to a dominant $L=2$ transition. Unfortunately,

TABLE XI. Experimental strengths for the effective *nucleon-nucleon* interaction at $\alpha^{-1}=1.0$ F obtained from (^{3}He,^{3}He′) $p_{1/2} \rightarrow s_{1/2}$, $d_{5/2}$ transitions.

Single-particle transition		Energy (MeV)	J^π, T	V_{00} (MeV) Wigner force	Serber force	Force III
$p_{1/2} \rightarrow d_{5/2}$	^{15}N	5.27	$\frac{5}{2}+,\frac{1}{2}$	70.3	72.4	64.9
		5.30	$\frac{1}{2}+,\frac{1}{2}$			
		5.27[a]	$\frac{5}{2}+,\frac{1}{2}$	91.1[b]	91.9[b]	80.9[b]
		7.15	$\frac{5}{2}+,\frac{1}{2}$	67.2	49.2	75.7
		7.56	$\frac{7}{2}+,\frac{1}{2}$	93.3	81.9	105.2
	^{14}N	5.10	2−,0	68.8	67.0	67.0
		5.83	3−,0	89.8	86.4	86.4
	^{13}C	3.85	$\frac{5}{2}+,\frac{1}{2}$	66.8	46.8	75.0
			Average	76.0±10	67.3±13	79.0±11
$p_{1/2} \rightarrow s_{1/2}$	^{15}N	7.30	$\frac{3}{2}+,\frac{1}{2}$	60.4	52.1	67.9
		8.31	$\frac{1}{2}+,\frac{1}{2}$	69.4	52.0	78.3
	^{14}N	4.91	0−,0	53.6	52.8	52.8
		5.69	1−,0	46.3	45.3	45.3
	^{13}C	3.09	$\frac{1}{2}+,\frac{1}{2}$	40.0	34.0	45.0
			Average	53.9±9	47.2±6	57.9±12

[a] The contribution from the 5.30-MeV, $p_{1/2} \rightarrow d_{5/2}$ transition is neglected.
[b] Not included in computing average strengths.

TABLE XII. Experimental strengths for the effective *nucleon-nucleon* interaction at $\alpha^{-1}=1.0$ F obtained from (^{3}He,t), $p_{1/2}\rightarrow d_{5/2}$ transitions.

Reaction	Energy (MeV)	J^π, T	Dominant L transfer	V_{01} (MeV)	V_{11} (MeV)
^{15}N(^{3}He,t)^{15}O	5.19[a]	$\frac{1}{2}+,\frac{1}{2}$	1	57.8	57.8
	5.24	$\frac{5}{2}+,\frac{1}{2}$	1,3		
	6.79[a]	$\frac{3}{2}+,\frac{1}{2}$	1	23.1	23.1
	6.86	$\frac{5}{2}+,\frac{1}{2}$	1,3		
	7.28	$\frac{7}{2}+,\frac{1}{2}$	3	39.7	39.7
	8.28	$\frac{3}{2}+,\frac{1}{2}$	1	···	15.5
^{14}N(^{3}He,t)^{14}O	6.28	(3−), 1	1	22.7	22.7
	6.79	(2−), 1	1,3	25.0	25.0
^{14}C(^{3}He,t)^{14}N	5.10[b]	2−, 0	1	···	31.0
	5.83[b]	3−, 0	3	43.0	43.0
^{13}C(^{3}He,t)^{13}N	3.51[b,c]	$\frac{3}{2}-,\frac{1}{2}$	0	18.2	18.2
	3.56[b]	$\frac{5}{2}+,\frac{1}{2}$	1,3		
			Average	32.8±12	30.7±11

[a] The contributions from these $p_{1/2}\rightarrow s_{1/2}$ transitions were included.
[b] DWBA calculations for these transitions are shown in Ref. 38.
[c] The angular distribution for the 3.51-MeV level was calculated using CK wave functions.

the 10.89- and 11.24-MeV levels are both weakly populated in the (^{3}He,t) reaction and therefore a meaningful comparison of the shapes of the experimental angular distributions could not be made (compare Fig. 17). However, approximate values were obtained for V_{01} which are given in Table X. It appears that these calculations do not strongly favor either candidate.

4. (^{3}He,^{3}He′) $p_{1/2}\rightarrow d_{5/2}$ Transitions

In principle, an $L=1$ ($S=1$) and/or $L=3$ ($S=0,1$) transfer is allowed for a $p_{1/2}\rightarrow d_{5/2}$ transition. However, since ($L0L0$) amplitudes are strongly enhanced for complex projectiles (see Sec. IV B2), the (^{3}He,^{3}He′) $p_{1/2}\rightarrow d_{5/2}$ transitions are all predicted to have dominant $L=3$ distributions [the $\frac{3}{2}+$ level in ^{15}N at 8.57 MeV is the only exception; it is restricted by the selection rules, Eqs. (14a), (14b), (14e), and (15), to be pure $L=1$ ($S=1$) and will be further discussed later]. The angular distributions for these $L=3$ transitions shown in Figs. 18 and 19 have a similar shape which is fairly well reproduced by the theoretical calculations. The values obtained for V_{00} are summarized in Table XI. Once again, they are relatively insensitive to the spin- and isospin-dependent terms in the effective interaction. The over-all agreement is very good considering the simple model which was assumed for the wave functions of these states. The average strengths obtained for V_{00} are somewhat larger than those computed earlier for $L=2$ transitions using the wave functions of CK; however, they are in better agreement with the values computed for $L=2$ transitions using simple j-j wave functions. Such results are consistent with those obtained from an analysis of $E3$ transition rates[64,65,74] (see discussion in Ref. 38).

TABLE XIII. Experimental strengths for the effective *nucleon-nucleon* interaction at $\alpha^{-1}=1.0$ F obtained from (^{3}He,t), $p_{1/2}\rightarrow s_{1/2}$ transitions.

Reaction	Energy (MeV)	J^π, T	V_{01} (MeV)	V_{11} (MeV)
^{15}N(^{3}He,t)^{15}O	6.79	$\frac{3}{2}+,\frac{1}{2}$	23.1	23.1
	6.86[a]	$\frac{5}{2}+,\frac{1}{2}$		
	7.55	$\frac{1}{2}+,\frac{1}{2}$	19.4	15.5
^{14}N(^{3}He,t)^{14}O	5.17	1−, 1	19.3	15.5
^{14}C(^{3}He,t)^{14}N	5.69	1−, 0	23.0	23.0
^{13}C(^{3}He,t)^{13}N	2.37	$\frac{1}{2}+,\frac{1}{2}$	12.0	9.5
		Average	19.4±3	17.3±5

[a] The contribution from the 6.86-MeV, $p_{1/2}\rightarrow d_{5/2}$ transition is included.

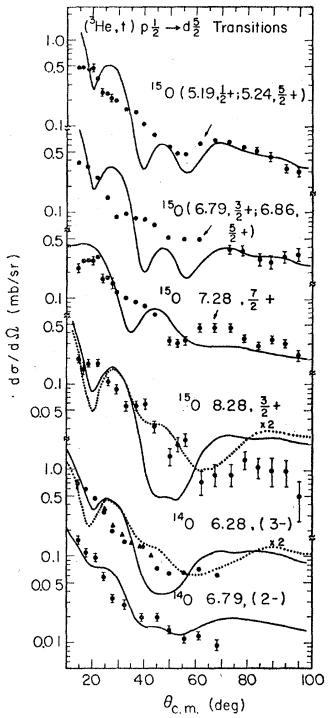

FIG. 20. Angular distributions for typical (^{3}He,t) $p_{1/2}\rightarrow d_{5/2}$ transitions. The solid curves are DWBA predictions obtained using j-j wave functions and the independent optical potentials given in Table VI. The dotted curves were calculated using unmodified optical potentials. The theoretical curves for unresolved levels were obtained by summing the predicted distributions for each level.

The 8.57-MeV, $\frac{3}{2}+$ level in ^{15}N is predicted to be a dominant $L=1$, $S=1$ transition. Theoretical fits are shown in Fig. 19 for both the modified and unmodified optical potential set; the latter appears to give a better over-all account of the experimental data. The values obtained for $V_{10}=V_{11}=22.0$ MeV using a Serber exchange mixture (see Table IX) can only be considered as upper limits since this level is also populated in the

[74] G. R. Bishop, M. Bernheim, and P. Kossanyi-Demay, Nucl. Phys. **54**, 353 (1964).

(α,α′) reaction[56] with approximately the same relative intensity as in the (³He,³He′) reaction (see Sec. IV C).

5. (³He,t) $p_{1/2} \rightarrow d_{5/2}$ Transitions

In contrast with the (³He,³He′) $p_{1/2} \rightarrow d_{5/2}$ transitions, the corresponding (³He,t) transitions are predicted to have mixed ($L=1$ and/or $L=3$) amplitudes ranging from almost pure $L=1$ to pure $L=3$ (compare Table XII). In general, the experimental angular distributions for these transitions have similar shapes (compare Fig. 20 and Ref. 18) while the theoretical curves vary, dependent upon the relative strengths of the $L=1$ and 3 components and do not reproduce experiment very well. (When two levels were unresolved, the theoretical curves were obtained by adding the contributions from each level.)

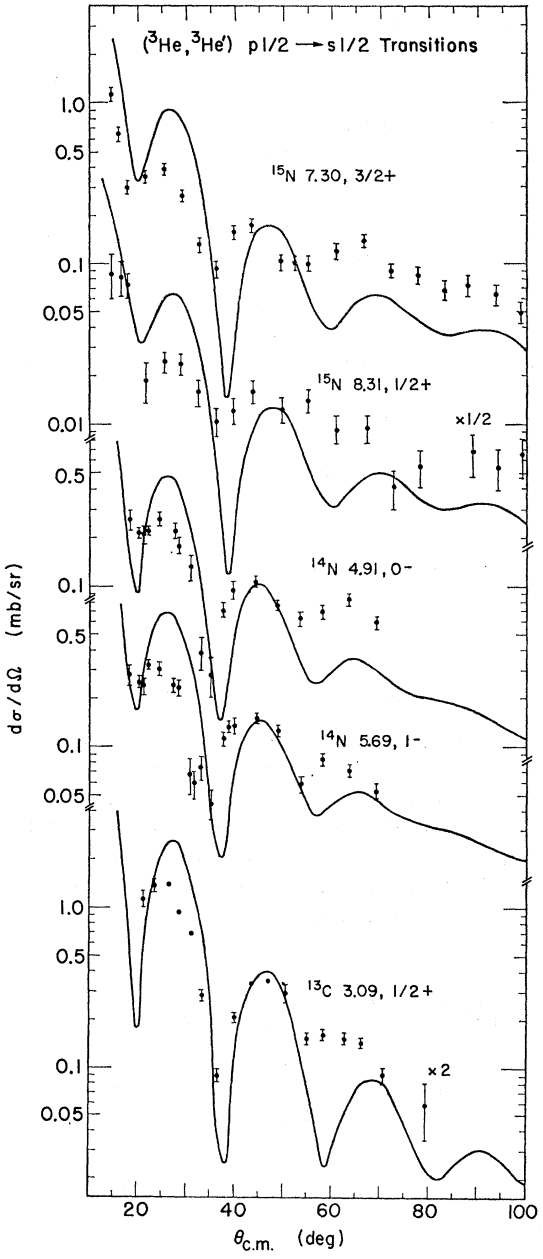

FIG. 21. Angular distributions for (³He,³He′) $p_{1/2} \rightarrow s_{1/2}$ transitions. The curves are DWBA predictions obtained using j-j wave functions, a Serber exchange mixture, and the independent optical potentials given in Table VI.

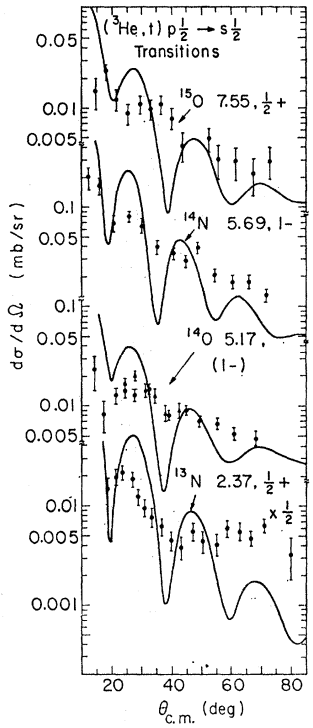

FIG. 22. Angular distributions for (³He,t) $p_{1/2} \rightarrow s_{1/2}$ transitions. The curves are DWBA predictions obtained using j-j wave functions and the independent optical potentials given in Table VI.

The curves shown in Fig. 20 for dominant $L=1$ transitions were calculated using both modified and unmodified optical potentials. Although the latter give a better fit to the data in the region $\theta_{c.m.} \cong 40°$–$60°$, both potential sets predict minima at $\theta_{c.m.} \cong 20°$ while the experimental data indicate maxima.

The values obtained for V_{01} and V_{11} are shown in Table XII; the relative agreement is not as good as that obtained for other single-particle transitions. In addition, the average strengths predicted for V_{01} [32.8±12 MeV] and V_{11} [30.7±11 MeV] are larger than the values required for $L=0$ transitions, indicating that the experimental cross sections for (³He,t) $p_{1/2} \rightarrow d_{5/2}$ transitions are also enhanced.

6. (³He,³He′) $p_{1/2} \rightarrow s_{1/2}$ Transitions

The experimental angular distributions for $p_{1/2} \rightarrow s_{1/2}$ transitions which are shown in Fig. 21 have more structure than those observed for other single-particle transitions. Theoretical calculations predict a well-defined oscillatory structure for these transitions; however, the fits obtained are not as good as those for (³He,³He′) $L=2$ and $L=3$ transitions.

TABLE XIV. A comparison of inelastic ^{3}He and α-particle scattering on $1p$-shell nuclei.

Dominant single-particle transition		Energy (MeV)	J^π, T	Integrated cross sections ($\theta_{c.m.}=20°$–$80°$) Absolute (mb) (^{3}He,^{3}He′)	(α,α')[a]	Relative (^{3}He,^{3}He′)	(α,α')	$G^2(L0L0)$ Relative (CK)	(jj)
$p_{3/2}\rightarrow p_{1/2}$	^{15}N	6.32	$\frac{3}{2}-,\frac{1}{2}$	1.70	3.80	1.31	1.56	1.03	1.0
	^{14}N	3.95	$1+,0$	1.30	2.44	1.0	1.0	1.0	1.0
		7.03	$2+,0$	1.61	2.59	1.24	1.06	0.91	1.0
	^{13}C	3.68	$\frac{3}{2}-,\frac{1}{2}$	4.25	12.10	3.27	4.95	2.78	1.5
		7.55	$\frac{5}{2}-,\frac{1}{2}$	4.29	12.60	3.30	5.16	2.66	1.2
		8.86	$\frac{1}{2}-,\frac{1}{2}$	0.289[b]	[c]	0.22	[d]	≈ 0	[e]
		11.84	$\frac{3}{2}-,\frac{1}{2}$	1.58	[c]	1.22	[d]	0.0017	0.3
	^{12}C	4.43	$2+,0$	22.9	41.1	17.6	16.8	10.15	4.0
						$\sigma_\alpha/\sigma^3_{He}=1.88$		$G_\alpha^2/G^{2^3}_{He}=1.78$	
$p_{1/2}\rightarrow d_{5/2}$	^{15}N	5.27	$\frac{5}{2}+,\frac{1}{2}$	2.02	7.38	1.34	1.42		1.69[f]
		5.30	$\frac{1}{2}+,\frac{1}{2}$						
		7.15	$\frac{5}{2}+,\frac{1}{2}$	0.308	0.591	0.204	0.114		0.402
		7.56	$\frac{7}{2}+,\frac{1}{2}$	1.91	9.16	1.26	1.76		1.28
		8.57	$\frac{3}{2}+,\frac{1}{2}$	0.174	0.516	0.115	0.10		[e]
	^{14}N	5.10	$2-,0$	1.10	3.68	0.728	0.71		1.25
		5.83	$3-,0$	1.51	5.18	1.0	1.0		1.0
	^{13}C	3.85	$\frac{5}{2}+,\frac{1}{2}$	1.43	4.18	0.947	0.807		1.12
	^{12}C	9.64	$3-,0$	4.19	22.7	2.78	4.38		···
						$\sigma_\alpha/\sigma^3_{He}=3.43$		$G_\alpha^2/G^{2^3}_{He}=1.78$	
$p_{1/2}\rightarrow s_{1/2}$	^{15}N	7.30	$\frac{3}{2}+,\frac{1}{2}$	0.659	3.23	1.58	1.98		2.0
		8.31	$\frac{1}{2}+,\frac{1}{2}$	0.109	0.747	0.262	0.458		0.25
	^{14}N	4.91	$0-,0$	0.416	1.63	1.0	1.0		1.0
		5.69	$1-,0$	0.464	1.82	1.11	1.12		2.0
	^{13}C	3.09	$\frac{1}{2}+,\frac{1}{2}$	0.690	3.41	1.66	2.09		1.5
						$\sigma_\alpha/\sigma^3_{He}=3.92$		$G_\alpha^2/G^{2^3}_{He}=1.78$	

[a] Harvey *et al.*, see Ref. 56.
[b] $\theta_{c.m.}=25°$–$80°$.
[c] Not reported in Ref. 56.
[d] These levels are populated in the (α,α') reaction at $E_\alpha=64.5$ MeV with approximately the same relative intensities as those observed in the (^{3}He,^{3}He′) reaction (see Ref. 38, 71).
[e] Forbidden in the j-j limit.
[f] The contribution from the 5.30-MeV, $\frac{1}{2}+$ level has been neglected.

Predicted values for V_{00} are summarized in Table XI. The over-all agreement is surprisingly good considering the simple j-j configurations which were assumed for these states. Since core polarization effects for $L=1$ transitions should be small, it is of interest that the average value obtained for V_{00} [47.2±6 MeV] is $\approx 10-20$ MeV smaller than those obtained for $L=2$ and $L=3$ transitions.

7. (^{3}He,t) $p_{1/2}\rightarrow s_{1/2}$ Transitions

In general, the levels which are populated in the (^{3}He,t) reaction by the promotion of a $p_{1/2}$ nucleon to the $s_{1/2}$ shell have much smaller cross sections than the other single-particle transitions to low-lying orbitals.[16,18] The angular distributions for these states which are shown in Fig. 22 have much less structure than is theoretically predicted. However, the values obtained

TABLE XV. A comparison of the experimental strengths for the effective *nucleon-nucleon* interaction at $\alpha^{-1}=1.0$ F obtained from the ^{14}N(^{3}He,^{3}He′)^{14}N and ^{14}N(α,α')^{14}N reactions at $E_{^3He}=44.6$ and $E_\alpha=40.5$ MeV, respectively.

Energy (MeV)	J^π	Dominant single-particle transition	V_{00} (MeV) (^{3}He,^{3}He′) Wigner force (jj)	(CK)	Serber force (jj)	(CK)	(α,α') Wigner force (jj)	(CK)
3.95	1+	$p_{3/2}\rightarrow p_{1/2}$	48.9	49.5	47.0	49.3	53.4	54.2
7.03	2+		59.9	63.7	50.9	52.2	54.6	58.0
4.91	0−	$p_{1/2}\rightarrow s_{1/2}$	53.6	···	52.8		58.5	
5.69	1−		46.3	···	45.3		45.4	
5.10	2−	$p_{1/2}\rightarrow d_{5/2}$	68.8	···	67.0		82.7	
5.83	3−		89.8	···	86.4		112.0	

for V_{01} [19.4±3 MeV] and V_{11} [17.3±5 MeV] (see Table XIII) are approximately equal to those for $L=0$ transitions, indicating that these transitions are not collectively enhanced.

C. Further Analysis

It is interesting to compare the effective *nucleon-nucleon* interaction required to fit the (^{3}He,t) and (^{3}He,^{3}He′) scattering data with those obtained from an analysis of available experimental data for the (α,α') and (p,p') reactions on 1p-shell nuclei. In particular, an analysis of the (α,α') reaction on several p-shell nuclei at $E_\alpha=40.5$ MeV[56] and the (p,p') reaction on ^{12}C at $E_p\cong46$ MeV[70] will be discussed below. Further, a comparison of the *effective* and *free* nucleon-nucleon interactions is presented.

1. *Comparison of* (^{3}He,^{3}He′) *and* (α,α') *Reactions*

The microscopic analysis of the (^{3}He,^{3}He′) reaction has shown that this reaction is in general very insensitive to the spin- and isospin-dependent terms in the effective interaction and, therefore, that the cross sections for strongly excited states are determined primarily by the ($L0L0$) amplitude. Since the (α,α') reaction is *only* dependent upon this term, a direct comparison of these two reactions populating the same final states could provide further evidence to support this conclusion.

An investigation of the elastic and inelastic scattering of 40.5-MeV α particles from several targets including ^{12}C, ^{13}C, ^{14}N, ^{15}N, and ^{16}O has been reported by Harvey

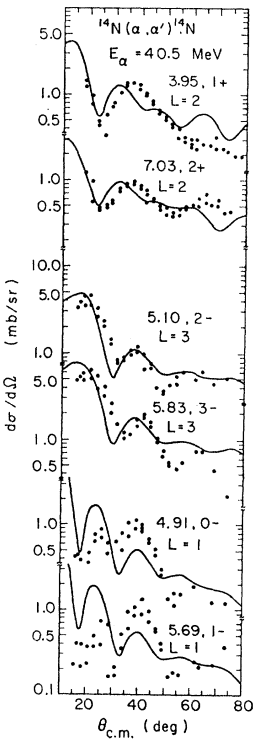

FIG. 23. Angular distributions from the ^{14}N(α,α')^{14}N reaction at 40.5 MeV. The solid curves are DWBA predictions obtained using the optical potential set M (see Table VI). Mixed CK wave functions were used for p-shell transitions, while simple j-j configurations were assumed for $p_{1/2}\rightarrow s_{1/2}$, $d_{5/2}$ transitions.

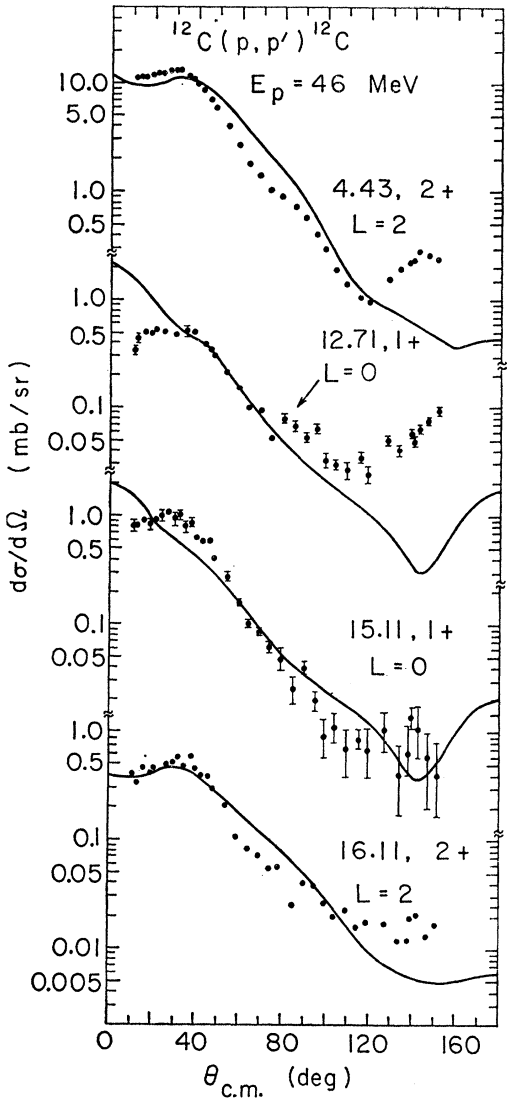

FIG. 24. Angular distributions from the ^{12}C(p,p')^{12}C reaction at $E_p=46$ MeV. The solid curves are DWBA predictions obtained using CK wave functions, a Serber exchange mixture, and the optical potential set $V1$ (see Table VI).

et al.[56] It was found that the angular distributions obtained from these reactions could also be characterized according to the particular shell-model transition involved. A comparison of the (^{3}He,^{3}He′) and (α,α') angular distributions indicates that the shapes are very similar, especially for $L=2$ and $L=3$ transitions; however, the magnitude of the (α,α') distribution is always approximately two to three times larger.

In Table XIV, relative integrated cross sections are compared for transitions observed in the (^{3}He,^{3}He′) and (α,α') reactions on several 1p-shell nuclei. The transitions have been grouped by specific shell-model transition, and in each case the cross sections have been arbitrarily normalized relative to the one single-particle transition in that group which was predicted to be the

TABLE XVI. A comparison of the experimental strengths for the effective *nucleon-nucleon* interaction at $\alpha^{-1}=1.0$ F obtained from the $^{12}C(^3He,^3He')^{12}C$, $^{12}C(^3He,t)^{12}N$, and $^{12}C(p,p')^{12}C$ reactions at $E_{^3He}=49.8$ MeV and $E_p=46$ MeV, respectively.

Energy (MeV)				(^{3}He,^{3}He′)				(^{3}He,t)		(p,p')			
				Wigner force		Serber force		Serber force		Wigner force		Serber force	
^{12}C	^{12}N	J^π, T	V_{ST}	(jj)	(CK)	(jj)	(CK)	(jj)	(CK)	(jj)	(CK)	(jj)	(CK)
4.43	···	2+, 0	V_{00}	92.7	59.0	92.0	59.0	···	···	137.0	87.1	127.0	86.9
12.71	···	1+, 0	V_{10}	···	···	10.6	27.0	···	···			9.4	23.7
15.11	0.0	1+, 1	V_{11}	···	···	10.2	24.3	10.1	24.4	···	···	10.8	26.1
16.11	0.96	2+, 1	V_{01}, V_{11}	···	···	29.4	46.1	29.3	45.8	···	···	20.2	31.6

most insensitive to spin- and isospin-dependent terms. The over-all agreement is excellent considering the simplicity of the comparison which is made. In addition, the nuclear structure factors $G^2(L0L0)$ are generally able to reproduce the observed trends in the relative magnitudes without actually carrying out a DWBA calculation.

If these reactions were only dependent upon the Wigner term V_{00}, then the relative cross sections to the same final states would be proportional to the square of the number of nucleons in the projectile. In Table XIV, it can be seen that the ratio of the integrated cross sections $\sigma_\alpha/\sigma_{^3He}$ ranges from 1.88–3.92 while the predicted value is 1.78.

In order to provide a better comparison for these reactions, a microscopic analysis was carried out for the $^{14}N(\alpha,\alpha')^{14}N$ reaction using the optical potentials shown in Table VI (a Yukawa potential with a range of 1.2 F was chosen for the effective *projectile-nucleon* interaction while a nonlocality range $\beta=0.25$ was assumed for the α particle). The results are shown in Fig. 23; the agreement between theory and experiment is reasonably good considering that no attempt was made to vary the parameters in order to improve the fits.

The values obtained for V_{00}, which have been converted to an effective nucleon-nucleon interaction at $\alpha^{-1}=1.0$ F [i.e., Eq. (8) was used[75] with $\gamma=0.329$ [5] and a range correction from 1.2 to 1.0 F was applied], are compared with those determined for the (^{3}He,^{3}He′) reaction in Table XV. Reasonably consistent results are obtained for the $p_{3/2}\rightarrow p_{1/2}$ and $p_{1/2}\rightarrow s_{1/2}$ transitions; however, the strengths required to fit the (α,α') $p_{1/2}\rightarrow d_{5/2}$ transitions are somewhat larger.

2. *Comparison of $^{12}C(p,p')^{12}C$ and $^{12}C(^3He,^3He')^{12}C$ Reactions*

An investigation of the $^{12}C(p,p')^{12}C$ reaction at $E_p=46$ MeV has been reported recently by Petersen *et al.*[70] These data were analyzed using both an extended version of the collective model which included spin and isospin oscillations[59,76] and also a microscopic description which made use of the distorted-wave impulse approximation (DWIA).[70] In the DWIA procedure, the projectile-nucleon interaction is replaced by the transition matrix for free nucleon-nucleon scattering.[1,29] Since the interaction is determined, the agreement with experiment provides a test of the nuclear wave functions used to describe the initial and final states, provided that the DWIA is valid at this energy. Fair agreement

TABLE XVII. A comparison of V_{ST} for various exchange mixtures used in nucleon-nucleon scattering and shell-model calculations.

$V(r_{12})=V_0(W+MP^x+BP^\sigma-HP^\tau)\exp(-\alpha r_{12})/\alpha r_{12}$, where $\alpha^{-1}=1.0$ F and $V_0=-135$ MeV ($A_0=1697$ MeV F^3).

Exchange mixture	W	M	B	H	A_{TE}	A_{SE}	A_{TO}	A_{SO}	V_{00}[a]	V_{10}	V_{01}	V_{11}
1. Serber	0.5	0.5	0.0	0.0	1.0	1.0	0.0	0.0	−50.6	16.9	16.9	16.9
2. Glendenning & Vénéroni[b,c]	0.4	0.4	0.1	0.1	1.0	0.6	0.0	0.0	−40.5	6.8	20.2	13.5
3. True[d]	0.406	0.406	0.094	0.094	1.0	0.625	0.0	0.0	−41.1	7.4	20.0	13.7
4. Ferrell-Visscher[e]	0.317	0.5	0.0	0.183	1.0	0.634	−0.366	0.0	−13.5	16.9	29.2	16.9
5. Rosenfeld[f]	−0.13	0.93	0.46	−0.26	1.0	0.6	−0.34	−1.78	0.0	0.0	13.5	31.0
Effective nucleon-nucleon interaction (^{3}He,t) (^{3}He,^{3}He′)									··· |60.2|	··· |(11–27)|	|20.6|	|16.5|

[a] All values of V_{ST} were calculated using a Yukawa potential with $\alpha^{-1}=1.0$ F and $V_0=-135$ MeV.
[b] A Yukawa with $\alpha^{-1}=1.13$ F and $V_0=-84$ MeV ($A_0=1523$ MeV F^3) reproduces the proton-proton scattering length and effective range (see Ref. 82).
[c] Used by Glendenning and Vénéroni (Ref. 3) in a microscopic analysis of (p,p') reaction on even nickel isotopes; radial dependence: Gaussian, $\beta^{-1/2}=1.85$ F $V_0=-52$ MeV ($A_0=1835$ MeV F^3).
[d] Used by True (Ref. 51) in a shell-model calculation for levels in ^{14}N; radial dependence: Gaussian, $\beta^{-1/2}=1.82$ F, $V_0=-52$ MeV ($A_0=1760$ MeV F^3).
[e] Used in a shell-model calculation of 0+ states in ^{16}O (see Ref. 81); radial dependence: Gaussian, $\beta^{-1/2}=1.732$ F, $V_0=-51.9$ MeV ($A_0=1502$ MeV F^3).
[f] A Yukawa with $\alpha^{-1}=1.37$ F and $V_0=-50$ MeV ($A_0=1615$ MeV F^3) gives the singlet-triplet separation for the deuteron (Ref. 83).

[75] The use of Eq. (8) for α particles involves a further approximation since this expression was derived specifically for mass-3 projectiles.
[76] G. R. Satchler, Nucl. Phys. **A100**, 481 (1967).

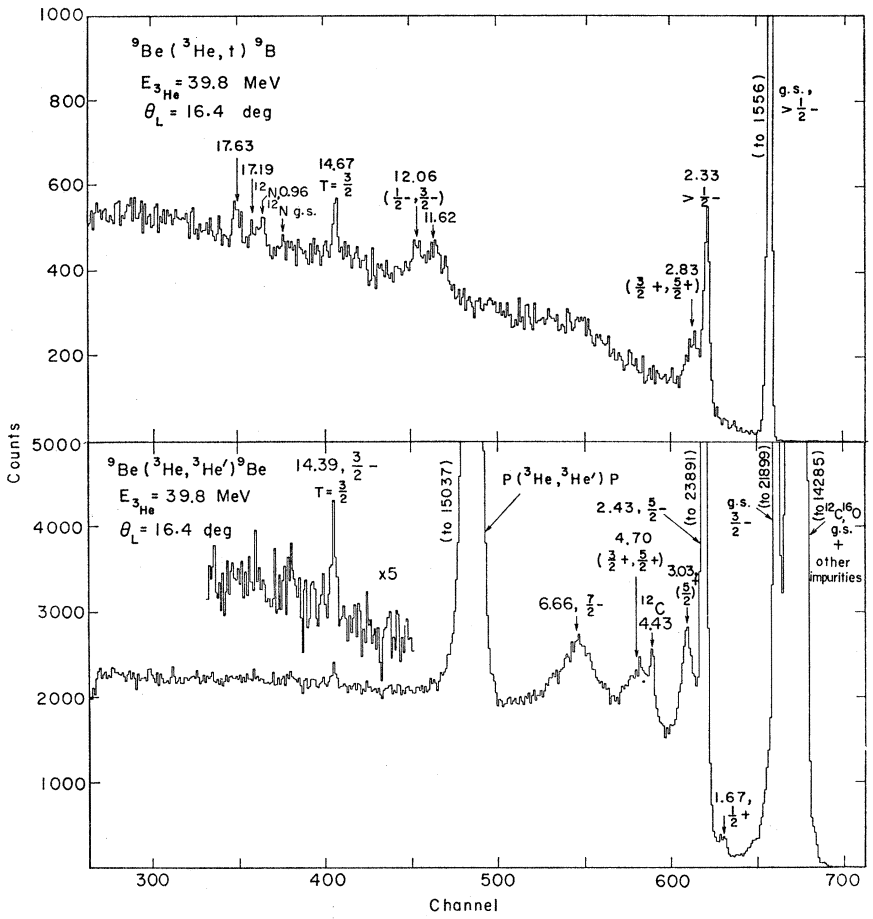

FIG. 25. Energy spectra of the ^{9}Be(^{3}He,t)^{9}B and ^{9}Be(^{3}He,^{3}He′)^{9}Be reactions at $E_{^3He}$=39.8 MeV and a scattering angle of 16.4°. The ^{9}B spectrum has been adjusted to align the mirror levels populated in both reactions.

was obtained when the wave functions of Gillet[77] were used to describe the levels of ^{12}C.

A comparison of the effective interaction required to fit the (p,p') data using the wave functions of CK with that required to fit the corresponding (^{3}He,^{3}He′) data should provide a test of the approximations made in determining the absolute strength of the effective nucleon-nucleon interaction from the scattering of complex projectiles [see Eq. (8)]. The calculations were performed using the optical parameter set $V1$ (see Table VI).[59] A Yukawa potential with a range of 1.0 F was chosen for the effective interaction, while the nonlocality range for a proton was assumed to be β=0.85 F.[78] The results are shown in Fig. 24; the theoretical angular distributions for restricted L=2 transitions are very similar to those obtained previously using the collective[59] and microscopic[70] models, while the calculations for the dominant L=0 distributions are still unable to fit the experimental data at small angles. The values obtained for V_{ST} are compared with those from the (^{3}He,^{3}He′) and (^{3}He,t) reactions in Table XVI. Fair over-all agreement is seen, indicating that the approximations which were made in the (^{3}He,^{3}He′) analysis are probably reasonable.

3. *Comparison of Effective and Free Nucleon-Nucleon Interaction*

It is interesting to compare the effective nucleon-nucleon interaction required to fit the (^{3}He,t) and (^{3}He,^{3}He′) scattering data with those used in simple shell-model calculations and those required to fit low-energy nucleon-nucleon scattering data. In order to facilitate this comparison it is helpful to briefly summarize the different forms in which a simple local interaction is generally used. Specifically, a simple local interaction with an arbitrary spin-isospin exchange mixture can be written in one of three equivalent forms given by

$$V(r_{12})=V_0[W+MP^x+BP^\sigma-HP^\tau]g(r_{12}), \quad (18)$$

where V_0 is in MeV; W, M, B, and H are constants; and P^x, P^σ, and P^τ are space, spin, and isospin exchange operators; or

$$V(r_{12})=V_0[A_{TE}P_{TE}+A_{SE}P_{SE}+A_{TO}P_{TO}+A_{SO}P_{SO}]g(r_{12}), \quad (19)$$

[77] V. Gillet and N. Vinh-Mau, Nucl. Phys. **54**, 321 (1964).
[78] F. G. Perey and B. Buck, Nucl. Phys. **32**, 353 (1963).

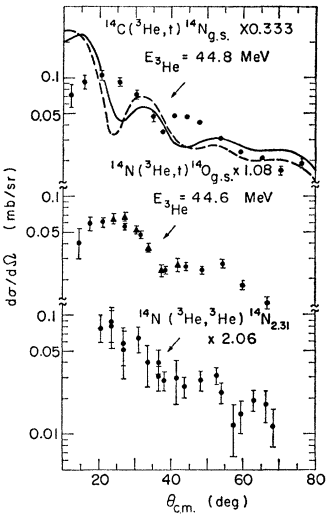

FIG. 26. Angular distributions for the $^{14}C(^3He,t)^{14}N$(g.s., 1+); $^{14}N(^3He,t)^{14}O$(g.s., 0+); and $^{14}N(^3He,^3He')^{14}N$(2.31-MeV, 0+) transitions. The cross sections have been corrected for detailed-balance, phase-space, and isospin-coupling factors. The solid and dashed curves are DWBA fits to the $^{14}C(^3He,t)^{14}N$(g.s., 1+) transition computed using CK and VF wave functions, respectively.

where A_{TE}, A_{SE}, A_{TO}, and A_{SO} are constants and P is a projection operator for the triplet-even, singlet-even, triplet-odd, and singlet-odd states; or

$$V(r_{12})=[V_{00}+V_{10}\sigma_1\cdot\sigma_2 +\tau_1\cdot\tau_2(V_{01}+V_{11}\sigma_1\cdot\sigma_2)]g(r_{12}), \quad (20)$$

where the V_{ST} are in MeV (i.e., V_0 is included in the values of V_{ST}). Expressions have been given elsewhere[3,4] which relate the coefficients of the individual terms for different parametrizations.

The coefficients predicted for several different exchange mixtures[3,51,79–81] are given in Table XVII. Although most of these potentials have been used in shell-model calculations, their strengths were chosen to fit low-energy nucleon-nucleon scattering data. All of these exchange mixtures, with the exception of the Serber force, have a singlet-even potential which reproduces low energy proton-proton scattering data[51,81–83] and possess a ratio of the singlet-even to triplet-even strengths approximately equal to that required to reproduce the binding energy of the deuteron.[3,51,83,84]

In order to compare the absolute values for V_{ST} arising from these exchange mixtures with those obtained in the present analysis, a Yukawa interaction with a range of 1.0 F and $V_0=-135$ MeV was chosen. This potential gives a volume integral, Eq. (7), of $A_0=1679$ MeV F^3(where $A_0\equiv A_{ST}$ and $V_0\equiv V_{ST}$) which is similar to those used previously for all exchange mixtures.

Since the Rosenfeld mixture is charge symmetric, while the Ferrell-Vischer exchange mixture was chosen to fit additional properties in ^{4}He and ^{16}O (see Ref. 81), the first three exchange mixtures listed in Table XVII should provide the best comparison with the present data. It can be seen that the values predicted for V_{01} [16.9–20.2 MeV] and V_{11} [13.5–16.9 MeV] are in very good agreement with the values of V_{01} [20.6 MeV] and V_{11} [16.5 MeV] obtained in the (^{3}He,t) analysis, while the values predicted for V_{00} [40.5–50.6 MeV] are somewhat lower than those observed in the (^{3}He,^{3}He′) reaction of $V_{00}\cong 60.2$ MeV. However, if one assumes that the enhancements due to core polarization effects are identical to the enhancements observed in the $E2$ matrix elements (i.e., 1.5–2.0, see Sec. IV B2),[20] then the value for V_{00} [60.2 MeV] is reduced to $\approx$30.1–40.2 MeV.

V. (^{3}He,t) AND (^{3}He,^{3}He′) REACTIONS POPULATING ANALOG FINAL STATES

A comparison of the (^{3}He,t) and (^{3}He,^{3}He′) reactions populating analog final states where $T_f=T_i+1$ was also of interest in these experiments. In general, these transitions were weakly populated; however, it was possible to observe the lowest $T=\frac{3}{2}$ levels in mass 9 and 13, the ground isobaric triad in mass 14, and several $T=1$ levels in mass 12.

Assuming the charge independence of nuclear forces, the ratio of the differential cross sections for these transitions is given by [see Eqs. (9) and (10)]

$$\frac{d\sigma(^3He,t)}{d\sigma(^3He,^3He')}=\frac{k_t}{k_{^3He}}\left|\frac{C_t'(T'T'1;P_i'-P_f')}{C'_{^3He'}(T'T'1;P_i'-P_f')}\cdot\frac{C_{^3He,t}(T_iT_f1;P_i-P_f)}{C_{^3He,^3He'}(T_iT_f1;P_i-P_f)}\right|^2 =\frac{2k_t}{k_{^3He}}\left|\frac{C_{^3He,t}}{C_{^3He,^3He'}}\right|^2. \quad (21)$$

This expression has ignored the differences between the t and ^{3}He energies, Coulomb potentials and internal wave functions in the exit channels.

A. $T=\frac{3}{2}$ Levels in Mass 9 and 13

The $^9Be(^3He,t)^9B$ and $^9Be(^3He,^3He')^9Be$ reactions were investigated at $E_{^3He}=39.8$ MeV; typical energy spectra are shown in Fig. 25. The well-known $\frac{3}{2}^-$, $T=\frac{3}{2}$ levels in ^{9}Be at 14.39 MeV and in ^{9}B at 14.67 MeV[85] are both weakly populated in these reactions. Isospin-coupling factors predict that the differential cross sec-

[79] R. S. Christian and E. W. Hart, Phys. Rev. **77**, 441 (1950).
[80] L. Rosenfeld, *Nuclear Forces* (North-Holland Publishing Company, Amsterdam, 1948), p. 234.
[81] R. A. Ferrell and W. M. Visscher, Phys. Rev. **102**, 450 (1956).
[82] M. A. Preston, *Physics of the Nucleus* (Addison-Wesley Publishing Company, Inc., Reading, Mass. 1962), p. 34.
[83] M. J. Kearsley, Nucl. Phys. **4**, 157 (1957).
[84] M. H. L. Pryce, Proc. Phys. Soc. (London) **A65**, 773 (1952).
[85] T. Lauritsen and F. Ajzenberg-Selove, Nucl. Phys. **78**, 1 (1966).

TABLE XVIII. A comparison of the (³He,t) and (³He,³He′) reactions populating analog states in the mass-14 triad.

Reaction	$E_{^3He}$ (MeV)	Cross sections ($\theta_{c.m.}=15°$–$80°$) Absolute (μb)	Adjusted[a] (μb)	(jj)	V_{11} (MeV) (CK)	(VF)
^{14}N(³He,t)^{14}O (g.s., 0+)	44.6	117±18[b]	126±19[b]	15.1	20.8	23.7
^{14}N(³He,³He′)^{14}N (2.31 MeV, 0+)	44.6	68±17[b]	140±35[b]	14.7	20.2	23.3
^{14}C(³He,t)^{14}N (g.s., 1+)	44.8	569±113[b]	189±37[b]	17.7	23.7	25.9

[a] See Fig. 26.
[b] Estimated errors include uncertainties in the absolute differential cross section plus statistical errors.

tions for $T=\frac{3}{2}$ levels populated in the (³He,t) and (³He,³He′) reactions should be essentially identical. Although angular distributions were not obtained for these transitions, the observed intensities were approximately equal at three forward angles between $\theta_L=13.4°$ and 16.4°.

The lowest $T=\frac{3}{2}$ levels in ^{13}C and ^{13}N were also weakly populated in the (³He,t) and (³He,³He′) reactions (compare Fig. 3). Unfortunately, an accurate comparison of the differential cross sections for these transitions could not be made due to poor statistics plus ^{12}C and hydrogen target impurities which made the observation of the $T=\frac{3}{2}$ level in ^{13}C impossible at forward angles.

B. ^{14}N(³He,t)^{14}O (g.s., 0+), ^{14}N(³He,³He′)^{14}N (2.31 MeV, 0+), and ^{14}C(³He,t)^{14}N (g.s., 1+) Reactions

The ^{14}N(³He,t)^{14}O (g.s.), ^{14}N(³He,³He′)^{14}N (2.31 MeV), and the inverse of the ^{14}C(³He,t)^{14}N (g.s.) reactions all correspond to transitions between identical initial and final states if charge independence is assumed. The experimental angular distributions which were obtained for these transitions are compared in Fig. 26; the magnitudes have been adjusted to correct for detailed-balance, isospin-coupling, and phase-space factors. In general, these transitions all have similar angular distributions while the adjusted integrated cross sections are approximately equal (compare Table XVIII). Although the DWBA calculations failed to fit the shapes of these distributions, the strengths required for V_{11} are in good relative agreement.

A similar comparison of the cross sections observed in the ^{14}N(p,n)^{14}O (g.s.), ^{14}N(p,p')^{14}N (2.31 MeV), ^{14}N(n,n')^{14}N (2.31 MeV), and ^{14}C(p,n)^{14}N (g.s.) reactions at $E_p\cong5$–14 MeV has been reported[86]; comparable results were obtained.

C. $T=1$ Levels in ^{12}C and ^{12}N

Several $T=1$ levels were populated in both the ^{12}C(³He,t)^{12}N and ^{12}C(³He,³He′)^{12}C reactions (compare Fig. 2). In addition, accurate angular distributions were obtained for the ground and first excited $T=1$ levels in ^{12}C and ^{12}N; these provide the best comparison of the (³He,t) and (³He,³He′) reactions populating analog final states. The two lowest $T=1$ levels in ^{12}C located at 15.11 and 16.11 MeV have well-known p-shell configurations with spins and parities 1⁺ and 2⁺, respectively. While the analogs of these levels in ^{12}N are presumed to be the ground and first excited (0.96 MeV) states,[41] the spin and parity of the latter have not been definitely determined. A comparison of corresponding (³He,³He′) and (³He,t) angular distributions for these levels is shown in Fig. 27; the (³He,³He′) distributions have been multiplied by 1.90 in order to correct for phase-space and isospin-coupling factors. In general the agreement is very good; however, the (³He,³He′) transitions appear to be approximately 10%

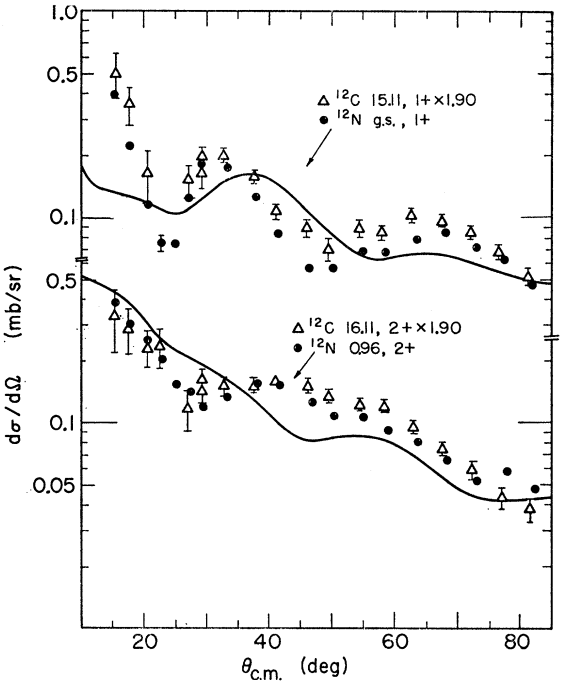

FIG. 27. Angular distributions for the ^{12}C(³He,t)^{12}N ground, 1+ and 0.96-MeV, 2+ states and for the ^{12}C(³He,³He′)^{12}C 15.11-MeV, 1+ and 16.11-MeV, 2+ states. The (³He,³He′) cross sections have been multiplied by 1.90 to correct for phase-space and isospin-coupling factors. The solid curves are DWBA fits to the (³He,t) transitions computed using mixed CK wave functions and the optical potential set F.

[86] J. D. Anderson, C. Wong, and V. A. Madsen, Lawrence Radiation Laboratory Report No. UCRL-50197, 1967 (unpublished).

TABLE XIX. $T=1$ levels in the mass-12 triad.

^{12}B			^{12}C			^{12}N	
J^{π} [a]	Energy[a] (MeV)	Level shift (keV)[b]	Energy (MeV)	$J^{\pi};T$	Dominant shell-model configuration	Level shift (MeV)[b]	Energy (MeV)	J^{π}
1+	0.0	...	15.11	1+;1	$(p_{3/2})_{3/2}{}^{7}p_{1/2}$	...	0.0	1+
2+	0.953	(+47)	16.11	2+;1	$(p_{3/2})_{3/2}{}^{7}p_{1/2}$	40	0.96	2+
2−	1.674	214	16.57	2−;1	$p^{7}s$	260	1.20	(2−)[c]
1−	2.62	470	17.26	1−;1	$p^{7}s$	500	1.65	
(≤3+)	2.72	60	17.77	0+;1	p^{8} [d]	230	2.43[c]	
(≤3+)	3.39	100	18.40[e]	(;1)[c]		190	3.10[c]	
2+	3.76	60	18.81	2+;1	p^{8} [d]	200	3.50[c]	
(1−)	4.30	210	19.2	1−,2−;1	$p^{7}(s,d)$			
3−	4.54	70[c]	19.58	(;1)[c]		230	4.24[c]	

[a] (See Ref. 42–44, 87).
[b] The level shifts are calculated relative to the ground-state multiplet.
[c] Tentative assignments made in the present work.
[d] Tentative assignments (see Ref. 40).
[e] A level observed previously in ^{12}C at 18.40 MeV is known to have $J^{\pi}=0-$; however, the isobaric spin of this level is unknown (see Ref. 45).

larger. Although this difference could be due to an incorrect background subtraction for the (^{3}He,^{3}He′) transitions, the detailed microscopic analysis suggests that this difference might be real.

First, DWBA calculations predict similar (differing in magnitude by $\leq 5\%$) single-particle cross sections $\sigma(j_1 j_2 L\theta)/k_f$ for the corresponding (^{3}He,t) and (^{3}He,^{3}He′) transitions. Therefore, the effects of the differing energies and Coulomb scattering in the exit channels are small. However, a comparison of the theoretical effective projectile-nucleon interaction for tritons or ^{3}He particles indicates that the internal wave functions of the complex projectiles may slightly affect the experimental ratio of these (^{3}He,t) and (^{3}He,^{3}He′) transitions. In particular, Eq. (8) predicts that the values for $\bar{V}_{ST}$ should be 1.07 times larger for (^{3}He,^{3}He′) transitions [i.e., the cross sections of (^{3}He,^{3}He′) transitions should be 1.15 times larger]. As a result, the observed increase in the experimental cross sections for these (^{3}He,^{3}He′) transitions can be accounted for, and the values obtained for V_{ST} from both reactions are in essentially perfect agreement (compare Table XVI). In addition, it can be concluded that the 0.96-MeV level in ^{12}N has a spin and parity of 2+ and is the analog of the 16.11-MeV level in ^{12}C.

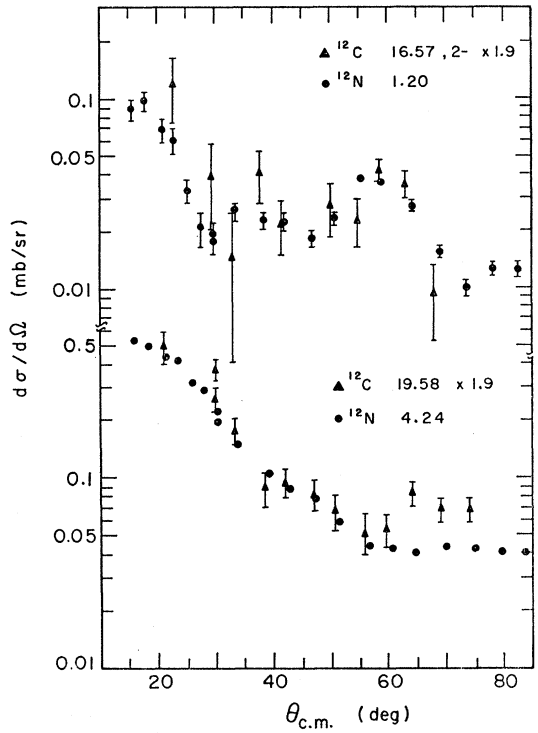

FIG. 28. Angular distributions for the ^{12}C(^{3}He,t)^{12}N 1.20-MeV, (2−) and 4.24-MeV states and for the ^{12}C(^{3}He,^{3}He′)^{12}C 16.57-MeV, 2− and 19.58-MeV states. The (^{3}He,^{3}He′) cross sections have been multiplied by 1.9 to correct for phase-space and isospin-coupling factors.

All $T=1$ levels observed in the ^{12}C(^{3}He,t)^{12}N and ^{12}C(^{3}He,^{3}He′)^{12}C reactions are summarized and compared with previous data[40–46] in Tables I and II. With the exception of the 17.26-, 17.77-, and 19.2-MeV levels, all well-known $T=1$ states in ^{12}C were observed up to an excitation energy of 20 MeV. In addition, all well-known levels in ^{12}N were observed with the exception of the 1.65-MeV level. Since the spins and parities of several $T=1$ levels in ^{12}C have been established, tentative assignments can be made for some excited states in ^{12}N by a comparison of the excitation energies (see also Ref. 41) and relative intensities—see Figs. 2 and 28—of the $T=1$ levels populated in the (^{3}He,t) and (^{3}He,^{3}He′) reactions. The results are summarized in Table XIX and also compared with known levels in ^{12}B.[42–44,87] Unfortunately, in most cases a meaningful comparison of the corresponding (^{3}He,t) and (^{3}He,^{3}He′) distributions could not be made due to poor statistics, large decay widths, and unknown contributions from $T=0$ levels (in ^{12}C). The individual assignments are discussed in detail in Ref. 38.

[87] L. F. Chase, Jr., R. E. McDonald, W. W. True, and E. K. Warburton, Phys. Rev. **166**, 997 (1968); J. W. Olness and E. K. Warburton, *ibid.* **166**, 1004 (1968).

TABLE XX. Average strengths for the effective *nucleon-nucleon* interaction at $\alpha^{-1}=1.0$ F obtained from (^{3}He,^{3}He′) and (^{3}He,t) transitions.

	(^{3}He,t) Present work				Previous work	
V_{ST}	$p_{1/2}, p_{3/2} \rightarrow p_{1/2}$ ($L=0$) (CK)	$p_{3/2} \rightarrow p_{1/2}$ ($L=2$) (CK)	$p_{1/2} \rightarrow d_{5/2}$ ($L=1,3$) (jj)	$p_{1/2} \rightarrow s_{1/2}$ ($L=1$) (jj)	(p,n)[a] $L=0$	(^{3}He,t)[b] $L=0$
V_{01}	20.6±0.4	42.4±5	32.8±12	19.4±3	19–26	31±6
V_{11}	16.5±1.1	42.4±5	30.7±11	17.3±5	$(V_{11}/V_{01}) \cong 0.6$–1.0	20±4

		(^{3}He,^{3}He′) Present work			(p,p') Previous work		
V_{ST}	Exchange mixture	$p_{3/2} \rightarrow p_{1/2}$ ($L=2$) (CK)	$p_{1/2} \rightarrow d_{5/2}$ ($L=3$) (jj)	$p_{1/2} \rightarrow s_{1/2}$ ($L=1$) (jj)	Target	Without core polarization[c]	With core polarization[d]
V_{00}	Wigner	60.3±6	76.0±10	53.9±9	^{7}Li	90	···
V_{00}	Serber	60.2±10	67.3±13	47.2±6	^{12}C	86.9[e]	···
V_{00}	Force III	54.2±5	79.0±11	57.9±12	^{18}O, ^{90,92}Zr, ^{208}Pb	≈200	≈80
		($L=0$)	($L=1$)				
V_{10}	Serber	≈27	≈22		^{89}Y, ^{90}Zr, ^{208}Pb	≈40[d]	
V_{10}	Force III	≈27					

[a] See Ref. 8, 10–12. [b] See Ref. 13, 14. [c] See Ref. 8, 10. [d] See Ref. 9. [e] See Sec. IV C2.

VI. CONCLUSIONS

A microscopic analysis of the (^{3}He,t) and (^{3}He,^{3}He′) reactions on 1p-shell nuclei has been carried out using a local potential with an arbitrary spin-isospin exchange mixture. Spectroscopic factors were calculated using the intermediate-coupling wave functions of Cohen and Kurath[19] for p-shell states while simple j-j configurations were assumed for the levels which were formed by promoting a $p_{1/2}$ nucleon to the $s_{1/2}$ or $d_{5/2}$ shell. A Yukawa interaction with a range of $\alpha^{-1}=1.2$ F was found to give the best over-all agreement for all transitions. The average strengths obtained for V_{ST} are summarized in Table XX and also compared with the results obtained in previous analyses of the (p,p'),[7–10] (p,n),[8,10–12] and (^{3}He,t) [13,14] reactions. In all cases, the values obtained for the effective *projectile-nucleon* interaction at $\alpha^{-1}=1.2$ F have been converted to an effective *nucleon-nucleon* interaction at $\alpha^{-1}=1.0$ F using the relationships given previously by Wesolowski *et al.*[14] and Johnson *et al.*[7]

Several interesting results were obtained from this analysis. First, the average values computed for V_{01} [20.6 MeV] and V_{11} [16.5 MeV] from the (^{3}He,t) $p_{3/2}$, $p_{1/2} \rightarrow p_{1/2}$, dominant $L=0$ transitions were in excellent agreement with those obtained previously in analyses of (p,n) $L=0$ transitions.[8,10–12] In addition, the strengths required to fit the (^{3}He,t) $p_{1/2} \rightarrow s_{1/2}$, $L=1$ transitions agreed well with these $L=0$ strengths. Second, the strengths required to fit the (^{3}He,t) $p_{3/2} \rightarrow p_{1/2}$, $L=2$ and $p_{1/2} \rightarrow d_{5/2}$, $L=1,3$ transitions were enhanced, while the experimental angular distributions for these transitions had less structure than those predicted by the theory. This suggests that core polarization effects or particle exchange could be contributing to the cross sections for these transitions. A similar effect has been observed for $L=2$ transitions in the (p,n) reaction.[11,12]

As expected, it was found that the transitions which were strongly populated in the (^{3}He,^{3}He′) reaction were generally insensitive to the spin- and isospin-dependent terms in the effective interaction. However, the absolute strengths obtained herein for V_{00} were much smaller than those required to fit the inelastic transitions observed in the (p,p') reaction on several heavier nuclei.[8] As a result, it can be concluded that core polarization effects are much less important for 1p-shell nuclei though, as noted above, they may still be contributing. Unfortunately, an accurate determination of the spin-dependent V_{10} term could not be obtained from these data. In particular, those (^{3}He,^{3}He′) transitions which were restricted to be pure $S=1$ were also populated in the (α,α') reaction with approximately the same relative intensity, indicating that other mechanisms such as multiple excitation also contribute significantly to the cross sections for these transitions.

Finally, it was shown (see Table XVII) that the effective interaction obtained in the present analysis is very similar to those used in simple shell-model calculations and those required to fit low-energy nucleon-nucleon scattering data.

ACKNOWLEDGMENTS

The authors wish to express their appreciation to Dr. Victor A. Madsen for the use of his DRC program and for additional valuable discussions. They also thank Dr. Dieter Kurath for providing his coefficients of fractional parentage and Dr. John C. Hardy for several helpful discussions.